GEOLOGICA CARPATHICA, FEBRUARY 2016, 67, 1, 41–68 doi: 10.1515/geoca-2016-0003

Evolution of the passive margin of the peripheral foreland basin: an example from the Lower Miocene Carpathian Foredeep (Czech Republic)

MICHAL FRANCÍREK and SLAVOMÍR NEHYBA

Institute of Geological Sciences, Faculty of Science, Masaryk University, Kotlářská 2, CZ- 611 37 Brno, Czech Republic; francirekmichal@seznam.cz, slavek@sci.muni.cz

(Manuscript received April 17, 2015; accepted in revised form December 8, 2015)

Abstract: The Karpatian deposits of the central part of the Carpathian Foredeep in Moravia, which are deeply buried under the Outer Western Carpathians, provide a unique opportunity to reconstruct the former evolutionary stages of this peripheral foreland basin and its paleogeography. A succession of three depositional units characterized by a distinct depositional environment, provenance, and partly also foreland basin depozone, have been identified. The first depositional unit represents a proximal forebulge depozone and consists of lagoon-estuary and barred coastline deposits. The source from the "local" crystalline basement played here an important role. The second depositional unit consists of coastline to shallow marine deposits and is interpreted as a forebulge depozone. Tidalites recognized within this unit represent the only described tide-generated deposits of the Neogene infill of the Carpathian Foredeep basin in Moravia. The source from the basin passive margin (the Bohemian Massif) has been proved. The third depositional unit is formed by offshore deposits and represents a foredeep depozone. The provenance from both passive and active basin margin (Silesian Unit of the Western Carpathian Flysch Zone) has been proved. Thus, both a stepwise migration of the foredeep basin axis and shift of basin depozones outwards/cratonwards were documented, together with forebulge retreat. The shift of the foreland basin depozones more than 50 km cratonward can be assumed. The renewed thrusting along the basin's active margin finally completely changed the basin shape and paleogeography. The upper part of the infill was deformed outside the prograding thrust front of flysch nappes and the flysch rocks together with a strip of Miocene sediments were superposed onto the inner part of the basin. The width and bathymetric gradient of the entire basin was changed/reduced and the deposition continued toward the platform. The basin evolution and changes in its geometry are interpreted as a consequence of the phases of the thrust-sheet stacking and sediment loading in combination with sea-level change.

Key words: Carpathian Foredeep, Late Burdigalian–Karpatian, peripheral foreland basin, Flysch Thrust Wedge, provenance.

Introduction

The geometry of a peripheral foreland basin is mainly a product of a complex dynamic balance between the orogenic loading, erosion and sedimentation, lithospheric flexural response to these processes, and sea-level changes (eustatic). DeCelles and Giles (1996) subdivided foreland basins into four distinct depozones: wedge-top, foredeep, forebulge, and backbulge. Several models were suggested to explain the relations between thrust loading, sediment supply, and basin shape (Flemings & Jordan 1989; Jordan & Flemings 1991), basin character and depozone migration (Heller et al. 1988; Catuneanu et al. 1998; Yang & Miall 2010). The principal data about the alternating phases of thrusting activity (orogenic loading) and tectonic quiescence (sediment loading) are provided by the study of either the proximal foredeep or the forebulge depozones (Flemings & Jordan 1989; Jordan & Flemings 1991; Sinclair et al. 1991; Crampton & Allen 1995; Plint 2000; Plint et al. 2001; Yang & Miall 2010; Leszczyński & Nemec 2014). However, as thrust movement propagates further and further onto the foreland, the foreland basin structure is "continually" modified as inner parts of the basin (proximal to active margin) are incorporated into the anticlinal thrust stack, and basin depozones are shifted further onto the foreland. This situation also means that foreland basins are continuously rearranged, and especially the most proximal parts of the basin's previous stages are poorly preserved. However such deposits have a potential to provide exclusive information about the basin's evolution and paleogeography. The results of subsurface exploration in eastern Moravia, where several deep wells penetrated the deposits of the Outer Carpathian Flysch Zone into the submerged part of the Carpathian Foredeep basin, offered such an opportunity. The proposed article aims to improve our understanding of the paleogeography and evolution of the Carpathian Foredeep basin during the Karpatian (Lower Miocene) based on detailed sedimentological and sedimentary-petrographical studies using data from 16 deep boreholes and 31 cores. "Alternative" lithological, sedimentological and paleontological results from the Carpathian Foredeep forebulge depozone have been published (Cogan et al. 1993; Hladilová et al. 1999; Nehyba & Šikula 2007; Zágoršek et al. 2012; Hladilová et al. 2014; Holcová et al. 2015).

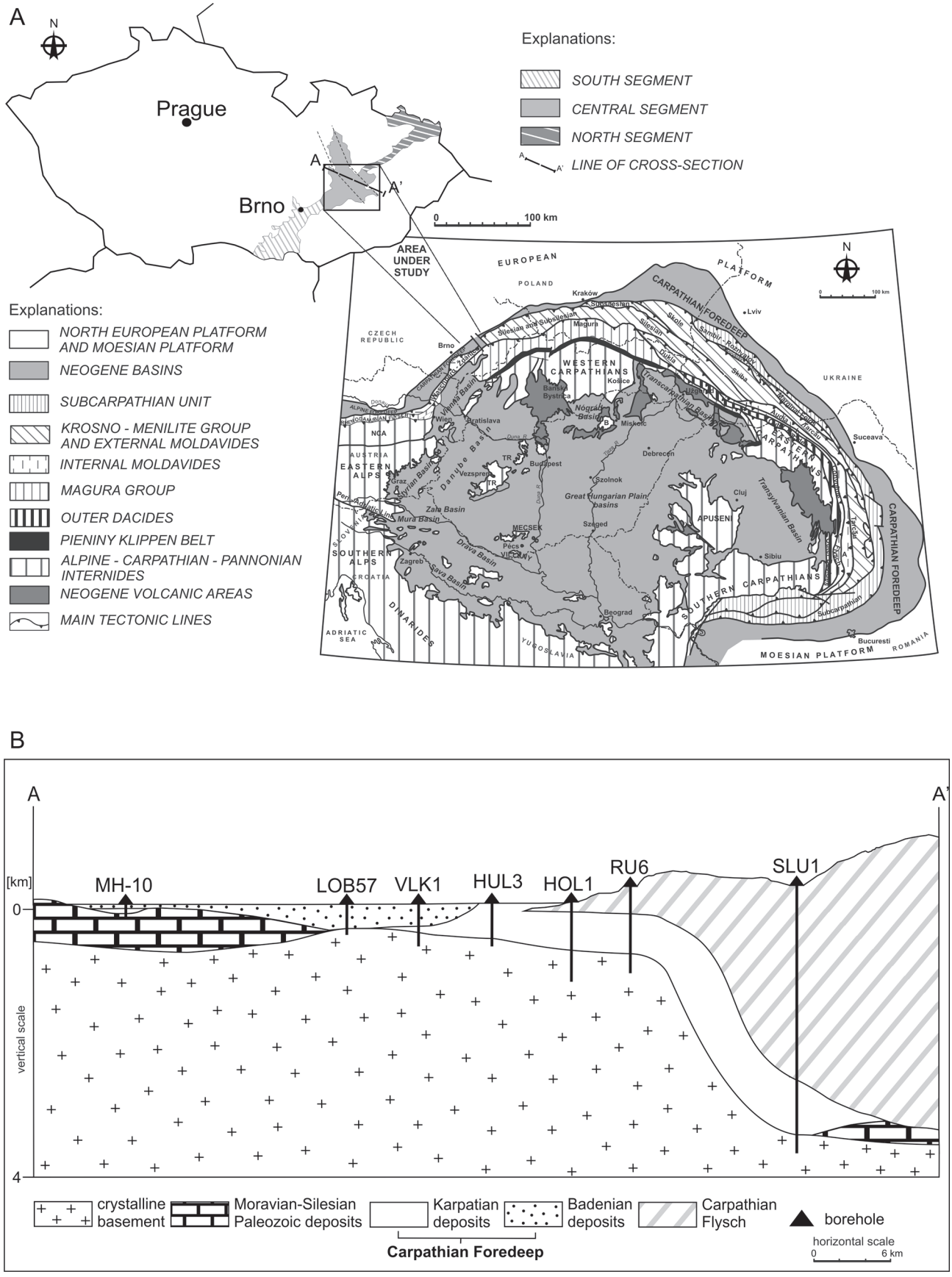

Fig. 1. A — Schematic map of the area under study and its position within the Carpatho-Pannonian region (modified after Kováč 2000), **B** — Geological cross-section (A–A') across the area under study.

Geological setting

The studied Neogene deposits belong to the western part of the Carpathian Foredeep, a peripheral foreland basin formed due to the tectonic emplacement and crustal loading of the Western Carpathian Thrust Front onto the passive margin of the Bohemian Massif (Nehyba & Šikula 2007) (Fig. 1A). The infill and basin architecture varies throughout the Carpathian Foredeep, local and regional unconformities are developed due to varying intensity and orientation of flexural loading and different geological and tectonic histories of the basement, along with a polyphase nature of the active basin margin and gradual change of its position (Brzobohatý & Cicha 1993; Eliáš & Pálenský 1998; Nehyba 2000; Nehyba & Petrová 2000; Krzywiec 2001; Kováč et al. 2003; 2004; Oszczypko et al. 2006; Nehyba & Šikula 2007).

The Moravian part of the Carpathian Foredeep was subdivided into three segments (i.e. southern, central, and northern ones), with partly different lithological and stratigraphical contents and depositional histories (Brzobohatý & Cicha 1993). The sedimentary infill of the basin is composed of deposits of Egerian to Badenian age; however only the Karpatian deposits (up to 1200 m thick) were identified in the studied area. The Karpatian depositional cycle is connected with a shift of the basin axis to the northwest due to continued thrusting of the Outer Carpathian Flysch Wedge (Brzobohatý & Cicha 1993), which also led to the overriding of the significant part of the Carpathian Foredeep by the flysch nappes (Fig. 1B) and partial incorporation of the basin infill into the nappes.

Seismic and borehole data showed that the pre-Miocene basement of the studied area is formed by crystalline rocks of the Brunovistulicum, limestones of the Moravian-Silesian Paleozoic and occasional Carboniferous clastic deposits of Drahany Highland unit (Kalvoda et al. 2003, 2008; Zágoršek et al. 2012; Hladilová et al. 2014). The basement generally dips southeastward, however the relief is very irregular. The basement is covered by Karpatian deposits, which were subdivided into the Mušov Member, the Nový Přerov Member and the Kroměříž Formation (Fig. 2). The Mušov Member is represented by grey marine mudstones with rich microfauna content (called "Schliers"). The Nový Přerov Member is formed of siltstones to mudstones with thin interbeds of fine- to medium-grained sandstones (the so-called "Sandy Schlier Formation") (Brzobohatý & Cicha 1993; Adámek et al. 2003). Mostly chaotic deposits of the Kroměříž Formation represent the final phase of the Karpatian depositional cycle (Benada & Kokolusová 1987; Adámek et al. 2003). Zádrapa (1979), described five facies of these Karpatian deposits (i.e. clastic, psammitic-pelitic, pelitic, pelitic-psammitic, and variegated ones). Thonová et al. (1987) divided them into three sections and Šikula & Nehyba (2006) described 6 well-log facies of these deposits. Detailed paleontological study of the Karpatian deposits in the area under study is missing.

The studied deposits are superposed by up to 4 km thick pile of the Western Carpathian Flysch Zone. In the Polish Carpathian Foredeep, this part located beneath the Carpathian nappes is described as inner foredeep (Oszczypko & Oszczypko-Clowes 2012, Waśkowska et al. 2014).

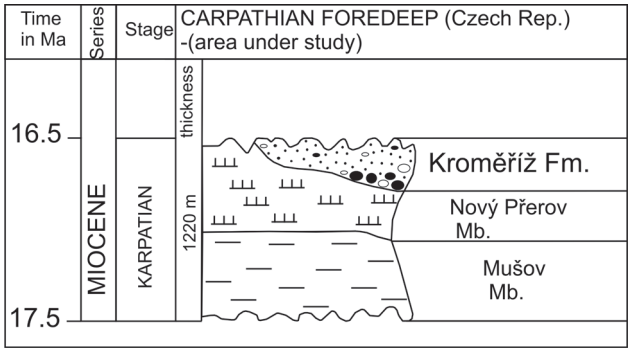

Fig. 2. Regional stratigraphic scheme of the Neogene of the Carpathian Foredeep in central Moravia (after Adámek et al. 2003).

Methods

The presented results are based on the study of the data from 16 boreholes. These boreholes are Bařice 1 (Bar 1), Gottwaldov 1, 2, and 3 (G 1, 2, 3), Holešov 1 (Hol 1), Hulín 1, 2, and 3 (Hul 1, 2, 3), Jarohněvice 1 (Jar 1), Kroměříž 1 and 2 (Kro 1, 2), Rataje 1 and 2 (Rat 1, 2), Roštín 1 and 2 (Ros 1, 2), Slušovice 1 (Slu 1), Tlumačov 1 and 2 (Tl 1, 2), and Vrbka 1 (Vr 1). The positions of the wells are presented in Fig. 3.

The lithofacies analysis is based on the sedimentological study of borehole cores, following the common rules of Miall (1989), Walker & James (1992), Reading (1996) and Nemec (2005). The quality and extent of the cores greatly varies, however they were mostly about 1 m long, exceptionally reaching up to 3 m. Therefore, further data provided evaluation of the available wire-line logs; "standard" wire-line techniques — spontaneous potential (SP), resistivity (Rag 2,12) and gamma-ray (gamma-API) (Rider 1986).

Maps of the thicknesses of deposits were created in the software Surfer 7 (gridding method). For the compilation of maps, the data from a slightly broader area (boreholes Kožušice 1, 4, Lubná 2, 4, Morkovice 1, 2, 4, Nítkovice 2, 4, 6, Rusava 1, 3, 5, 6 and Stupava 1, 2) have been used.

Provenance analysis is based on the petrographical studies of core samples. The framework grains were point counted in 27 thin sections according to the standard method (Dickinson & Suczek 1979; Dickinson et al. 1983; Ingersoll 1990; Zuffa 1980; 1985). The entire rock geochemistry was evaluated at ACME Laboratories in Vancouver, Canada (57 analyses).

The chemical index of alteration (CIA) is commonly used (Nesbitt & Young 1982; Nesbitt & Young 1989; Fedo et al. 1995; Nesbitt et al. 1996; von Eynatten et al. 2003; Li & Yang 2010). Due to the absence of CO_2 data and different contents of carbonate, a precise correction for the carbonate CaO* was difficult. The correction is based on the indirect method, in that it is necessary to deduct the mole fraction of P_2O_5 (apatite) from the mole fraction of CaO*. The value of CaO* is accepted if the remaining mole fraction of $CaO<Na_2O$. However, if $CaO>Na_2O$ then CaO* corresponds to $CaO=Na_2O$ (McLennan 1993).

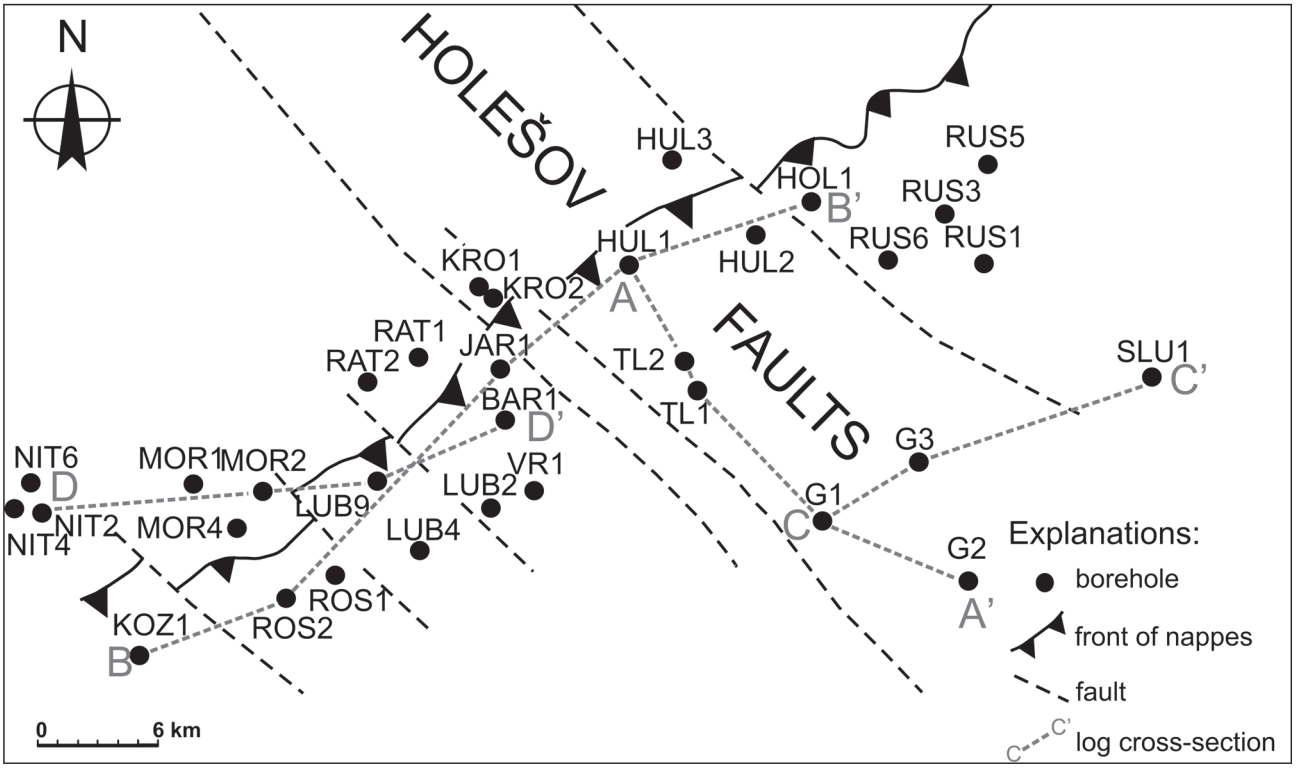

Fig. 3. Location of the studied boreholes and log cross-section (Fig. 5A-D).

Heavy minerals were studied in the 0.063–0.125 mm grain-size fraction in 33 samples. The data of the heavy minerals assemblages were obtained from the archives of the MND Group. The electron microprobe analysis of garnet (336 grains of Karpatian deposits and 15 grains of the crystalline basement) and rutile (103 grains) was performed with a CAMECA SX electron microprobe analyser in the Faculty of Science, Masaryk University, Brno, Czech Republic. The following analytical conditions were used: 15 kV accelerating voltage, 20 nA beam current, beam diameter 2–5 μm. Garnet and rutile grains were analysed in their centres. Fe_2O_3 and FeO were calculated from stoichiometry. The formula was standardized to 12 oxygens and 8 cations. Garnets and rutiles were studied in the sandstones and siltstones of the boreholes G 1, G 2, Hol 1, Hul 2, Kro 1, Kro 2, Ros 1, Ros 2, Slu 1, Tlu 1 and Tlu 2.

Results

Facies analysis

Individual lithofacies were identified according to grain size and sedimentary structures. Recognized lithofacies are briefly described in Table 1 and can be followed in Fig. 4. Lithofacies can be grouped into fine-grained, heterolithic, sandstone, and coarse-grained categories based on the dominant grain size. Lithofacies have been combined, based on their spatial grouping in cores into five facies associations (FA).

The FA1 is formed by the dominant lithofacies M1 and less frequent M2. The FA1 is located on the base of the depositional succession and is situated on the western and central part of the studied area.

The FA2 is composed mostly of lithofacies S3, S1, and S4 and less commonly S2, S6, H3, and G1. Sandstone facies strongly dominates (forming 95.4 %), whereas gravel and heterolithic facies form only a few percent of the succession. The FA2 is substituted for FA1 and is therefore located on the base of succession or above FA1; it is situated in the western part of the area.

The FA3 is formed dominantly by sandstone lithofacies S4, S2, S1, and S5, while fine-grained M1 and M2 and heterolithic H1 and H3 ones are less common. The occurrence of individual lithofacies categories varies in individual wells (sandstone lithofacies represent 47.1–51.1 %, heterolithic ones 20.4–39.0 %, and fine-grained ones 12.9–28.4 %). The occurrence of herringbone cross-lamination (facies H3) within the upper part of FA3 has been recognized in some wells (G 1, G 2). The FA3 is superimposed on FA1 and FA2 and is located in the western part of the area.

The FA4 is represented dominantly by heterolithic lithofacies H1, H2, and H3 (forming 46.1–66.2 %), whereas sandstone lithofacies S1, S2 and S5 (17.6–29.8 %) and fine-grained lithofacies M1 and M2 (4.1–36.4 %) are less common. The FA4 is situated above FA1 in the central part of the area.

The FA5 is formed predominantly by fine-grained lithofacies M1 (50–87 %); heterolithic lithofacies H1 and H2 are less common (13–38.8 %) and facies M2 is only occasional. The FA5 is situated above FA1 or FA4 in the central part of

Table 1: Description and interpretation of lithofacies.

Symbol	Description	Interpretation
M1	Dark grey silty mudstone, massive to planar laminated with a occasional occurrence of milimeters thick (max. 3 mm) mostly discontinuous laminas of very fine-grained sand (with glauconite). Silt admixture is irregularly distributed. Abbundant content of coalified plant detritus, which can be grouped into thin laminas. The bed thickness is over 20 cm, sharp erosional base. Varied occurrence of light mica and pyrite. Exceptional presence of foraminifera tests.	Dominant deposition from suspension, occasionally disturbed by rapid sediment delivery (upper flow regime, storm activity, mass flows). The absence of infauna, high content of plant debris point to rapid deposition and/or oxygen deficiency.
M2	Dark grey massive to poorly visible planar laminated silty mudstone, bioturbated (the bioturbation index varies). Typical is an occurrence of small (Ø max. 1cm) subhorizontal tunnels with rounded or elliptical shape, filled with light grey very fine sandstone. Admixture of coalified plant detritus and shell debris (molluscs, foraminifera) is typical, similarly presence like presence of glauconite, white mica and pyrite. The bed thickness ranges from 16 to 30 cm. The tops are sharp and erosional.	Deposition mostly from suspension, suitable conditions (oxygen content, sediment delivery, etc.) for the bottom colonization, basinal environment.
H1	Dark grey or dark brownish grey silty mudstone with occasional occurrence of laminas (mostly discontinuous) or irregular thin lenses of light grey very fine to fine-grained sandstone (max. about 1 cm thick) – lenticular bedding. The variable content of plant debris, fine mica and shell fragments. The bed thickness ranges from 5 cm to 1 m. The bases and tops are both flat/sharp.	The dominant deposition from suspension occasionally alternates with traction current deposition. Inner shelf deposits (storm activity).
H2	More or less regular alternation of laminas to thin beds (up to 2 cm thick) of dark grey silty mudstone and beds (mostly 2–5 cm, max. 10 cm thick) of light grey very fine- to fine-grained sandstone. Ripple cross lamination or planar lamination preserved in thicker beds of sandstone. Thinner beds are typical by planar lamination. Wavy bedding to rhytmites. Parting lineation. Very rare occurrence of foramineferal tests, fish remnants, glauconite and plant fragments Abundant occurrence of synsedimentary deformations (loading, pillow and flame structures, casps) and sole marks. Occurrence of plant debris. Erosional bases and tops. Low bioturbation index.	The rapid (rhytmic) alternation of deposition from traction currents and deposition from suspension. Rapid deposition, water escape deformation to fluidization. Inner shelf deposits (storm activity) and/or tidalites.
H3	Light grey, micaceous, fine- to medium-grained sandstone with laminas and flasers of dark silty mudstones (0.3 to 1.5 cm thick) – flasser bedding. Well preserved ripple cross lamination in sandstones, sometime evident herringbone cross-lamination. Mudstone laminas are often deformed (undulated, continuous lamina). The thickness of beds ranges from 7–27 cm. The bases are flat and erosional. The tops are commonly sharp and erosional. Parting lineation of whitish mica, rare occurrence of foraminefera tests, spongies and glauconite.	Rapid alternation of sandstone deposition from traction current and mudstone deposition from suspension. In some cases documented alternation of flow directions (tidal activity), rapid deposition.
S1	Light grey, whitish grey, fine- or fine to medium grained sandstone, micaceous with plane paralel lamination, well sorted. Bed thickness up to 20 cm. Sharp erosive base (especially if superposed to fine grained M facies). Varied occurrence of plant fragments (exceptionally up to 0.5 cm in diameter). Locally strings of small (about 2 cm) quartz pebbles (one grain thick).	Upper flow regime – upper shoreface deposits, pebble strings point to storm activity.
S2	Light grey to whitish grey, fine to medium grained sandstone, micaceous. Structureless due to intense bioturbation which complitely obliterated the primary structures. Rare occurrence of small plant debris and fragments of organic rich mudstone. Exceptionally 3 cm lense of quartzose gravellite (matrix supported – sand matrix).	Lower shoreface deposits – admixture of coarser clasts points to storm activity.
S3	Light grey locally green-grey, micaceous, fine or medium-grained sandstone, cross stratified (ripple cross lamination), relative well sorted, exceptional occurrence of small rounded quartz pebbles (up to 2 cm). The set thickness range between 15–20 cm, thickness of cosets is about 40 cm. Sharp bases and tops. Sometime relative low degree of bioturbation.	Traction current, lower flow regime, unidirectional(?) flow, high energy conditions, foreshore to upper shoreface deposits.
S4	Light grey locally green grey, fine grained sandstone, micaceous, ripple cross laminated. Generally well sorted, but locally "nests" or scattered granules to small pebbles (1–2 cm in diameter) of well rounded whitish quartzes. Sharp base locally (if superimposed to M or H facies) loading structures. Varied occurrence of shell debris and plant debris.	Lower flow regime, traction currents, shoreface deposits.
S5	Light grey localy green grey, micaceous, fine or medium-grained sandstone, undulated lamination to hummocky cross-stratification (HCS) or its variations. Typically planar lamination along the base, transition to undulated inclined/ripple lamination and finally planar lamination. Upper interval of planar lamination is typical with alternation of relative coarser and finer laminas. Irregularly inclined bases of sets. Relative common was fining upward trend (both reduction of the grain size and admixture of silt towards the top of sets). Irregular fragments (up to 2 mm) of mudstone sometime along the base. Occurrence of light mica. The bed thickness usually several cm up to 15 cm. Both the bases and tops are sharp and erosional. Varied but mostly low presence of shell debris, pyrite, glauconite and plant fragments.	Combined action of current and wave, result of storm activity. Deposition below the fairweather wave base - lower shoreace to inner shelf. Relative low thickness and preservation of limited part of the storm succession (Dott, Bourgeois 1982) point to inner shelf conditions.
S6	Dark grey, fine to medium grained micaceous sandstone with abundant presence several mm thick continuous laminas of coalified plant detritus or coal and mudstone intraclasts. Typical is occurrence of pyrite. Facies recognized very exceptionally.	Intense and periodic delivery of plant material – prohibited deposition (backshore, lagoon, floodplain).
G1	Light grey very coarse grained pebbly sandstone, gravellite or fine pebble conglomerate. Subagular to angular clasts of deeply weathered and kaolinized granitoids dominate within the pebbles. Well rounded quartzes (3 cm in diameter) are less common. Only fragments of core preserved.	Partly short transport from adjacent crystalline basement, proximity to terrestrial conditions.

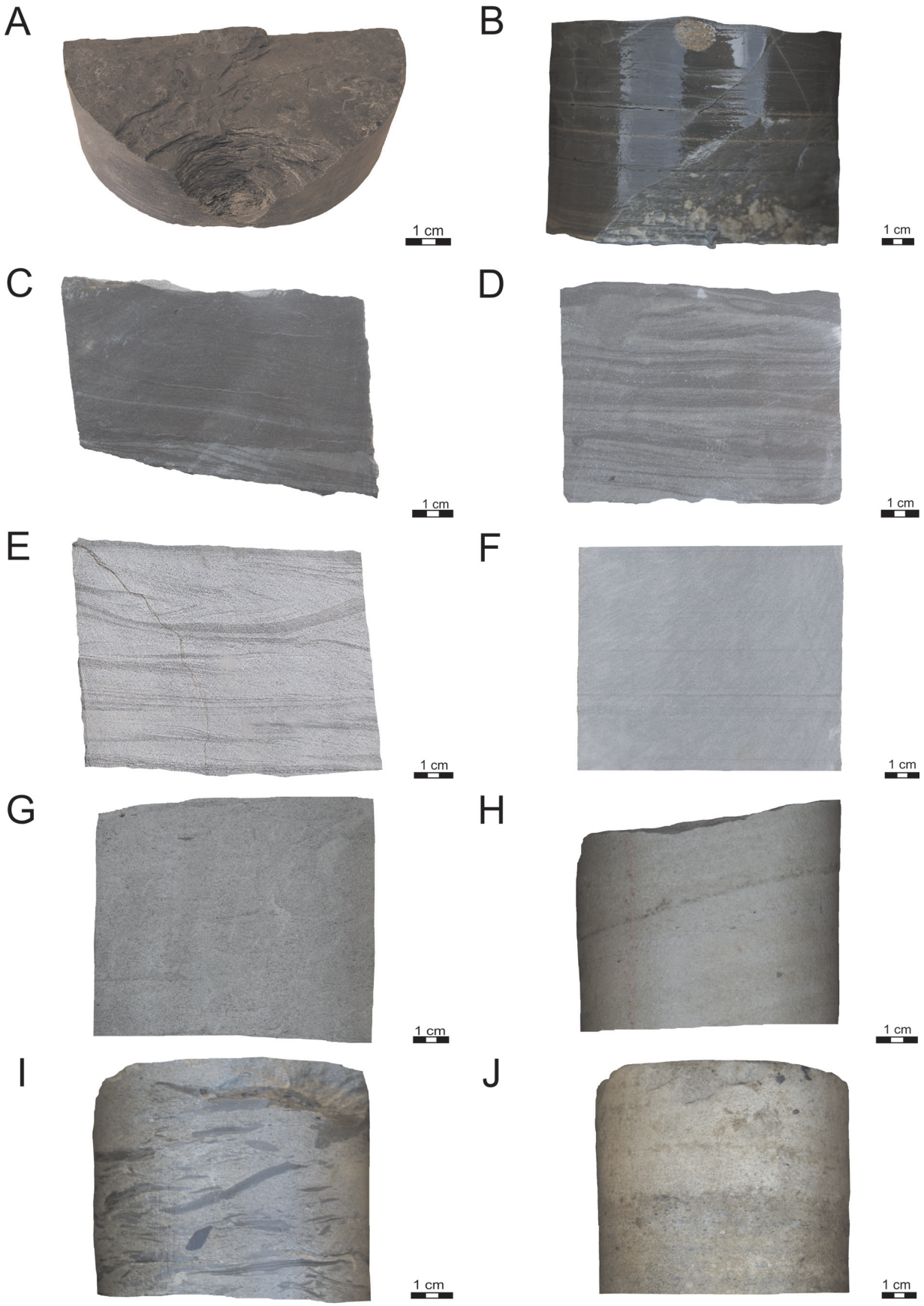

Fig. 4. Selected examples of lithofacies. **A** — facies M1, **B** — facies M2, **C** — facies H1, **D** — facies H2, **E** — facies H3, **F** — facies S1, **G** — facies S2, **H** — facies S3, **I** — facies S6, **J** — facies G1.

the area or on the base of the basin succession at the eastern margin of the basin.

The lithofacies content of the FA1–5 can be compared with the shape of well logs and combined with their areal position. Thus three depositional units (DU) can be identified. Log cross-sections with spatial arrangement of these DU are presented in Fig. 5A–D.

The DU I is located along the base of the basin fill. The thickness ranges from 3 to 57 m (Fig. 6) and is greatest around the borehole Vr 1. The whole unit reveals a broadly lenticular shape, extended predominantly in the SW–NE direction. Two subunits (DSU) with different facies content and areal position can be recognized. The more common subunit IA is represented by the FA1 and is developed in the central part of the studied area. The subunit IA reveals a curved funnel shape prolonged in the NW–SE direction (Fig. 7A) with thickness ranging between 3 and 40 m. The subunit IA was recognized in boreholes Bar 1, G 1, 2, 3, Hul 1, Jar 1, Kro 1, 2, Rat 2, and Tl 1, 2 with a typical bell-shape of the gamma and Sp logs (fining-upward trend).

The less common subunit IB was recognized in boreholes Hol 1, Hul 2, 3, Ros 2, Slu 1, and Vr 1 and is represented by the FA2. A generally blocky shape of gamma and Sp logs is typical. However, the lower part of this subunit seems to be less monotonous (slightly irregular and funnel shaped of logs), pointing to a coarsening-upward trend and alternation of sandstone and mudstone beds. The upper part reveals a more monotonous blocky shape and monotonous lithology. The subunit IB occurs along the southwest and northeast margins of subunit IA (Fig. 7B) with a maximum thickness of 54 m. The interfingering of subunits IA and IB was recognized in wells G 3, Ros 2.

The DU II is situated in the southeast part of the area (recognized in boreholes G 1, 2, 3, Ros 1, 2, Slu 1, Tl 1, 2, and Vr 1), where it covers either subunit IA or subunit IB. The total thickness of DU II ranges from 20 to 426 m (Fig. 8) with the maximum around the borehole G 1. The unit is extended in the SW–NE direction, parallel with the thrust front. The DU II mostly consists of FA3, FA4, and FA5 and generally reveals a multiple repetition of a funnel-shape (coarsening-upward trend) of well logs. Up to four of such trends/cycles were recognized within the succession of the DU II with thicknesses of each one ranging from 12 to 55 m. Commonly a succession of FA5–FA4–FA3, were observed from the base to the top of the cycle; however an incomplete succession is commonly preserved. The lower fine-grained part (FA5 and FA4) is significantly thicker (about 15 m) than the sandier part (FA3). The lowermost cycle usually reaches the greatest thickness.

The DU III is either superposed to DU II (southeast part of the area) or directly overlaps the deposits of DU I (northwest part). The DU III is described in all studied boreholes except for borehole G 1. The unit occurred as a continuous tabular belt prolonged in the SW–NE direction (parallel to the thrust front) and inclined towards the southeast (where tectonic removal of the unit is supposed). The thickness of DU III ranges between 200 and 1000 m (Fig. 9) and increases towards the fronts of nappes. The log curves mostly have a monotonous flat or slightly irregular shape, which, together with values of Rag, Sp, and gamma, indicates dominantly fine-grained content, while sandstone interbeds are rare and thin. The interpretation is confirmed by cores, where FA5 was recognized. Strongly tectonically deformed (cracks, slickenslides, etc.) deposits of DU III have been identified mainly within the borehole Vr 1.

Interpretation

The FA1 is interpreted as lagoonal/estuarine deposits which are faunistically poor and lacking the presence of features of the open sea (Dalrymple et al. 1992; Sacchi et al. 2014). The FA2 is determined as backshore-shoreline (strandplain?) deposits (Wright et al. 1979; Walker & Plint 1992). The FA3 is interpreted as foreshore to lower shoreface deposits. Herringbone cross-lamination points to tidally influenced deposition (tidal flats — Reineck & Singh 1973). A mudflat and mixed-flat depositional environment is supposed for a part of the FA3 (FitzGerald et al. 2012; Reynand & Dalrymple 2012). The FA4 is interpreted as deposits of the lower shoreface and the transitional zone to the inner shelf (Duke 1985; Duke et al. 1991). The FA5 is interpreted as deposits of the inner and outer shelf.

The lithological infill of DU I can be compared to the Mušov Mb. (Adámek et al. 2003). The DU I deposits are paleontologically depleted. The remains of Teleostei and fragments of skeletons and teeth of epipelagic species (*Lepidopus*) were described (Thonová et al. 1987).

The areal extent and sedimentary infill of the subunit IA point to the important role of basement morphology on its formation, probably due to reactivation of the basement faults in the compressive regime of the early stages of foreland basin evolution (similarly see Gupta 1999; Krzywiec 2001; Oszczypko et al. 2006; Nehyba & Roetzel 2010). Major faults trend NW–SE, downthrowing mainly to the SW. We can speculate about the existence of a paleovalley, trending in the NW–SE direction. The role of basement tectonics is also supported by the preservation of the Paleozoic deposits within this paleovalley surrounded by crystalline rocks on its margins. The depositional subunit IA could represent an "Early transgressive systems tract" (Koss et al. 1994; Shanley & McCabe 1994) due to localized preservation, dominant vertical accretion, and its position below the major transgressive surface.

The subunit IB is connected with the marine transgression on the distal northwest margins of the basins. The sedimentary infill might be connected with the distal part of a valley (Cattaneo & Steel 2003) adjacent to the marine basin (to the southeast) with a proximity to the terrestrial environment (to the northwest?). A highly varied morphology of the coastal area with a steep and irregular relief along the margins of the paleovalley and the flatter and more depressed relief in its central part of valley is supposed. Such a situation could lead to more rapid and further ingression of the marine flooding into the foreland through the valley. Numerous small basement elevations (forming shoals, small islands or intrabasinal highs) and a highly irregular pattern of the shore favour significant differences in the slope and width of the coastline

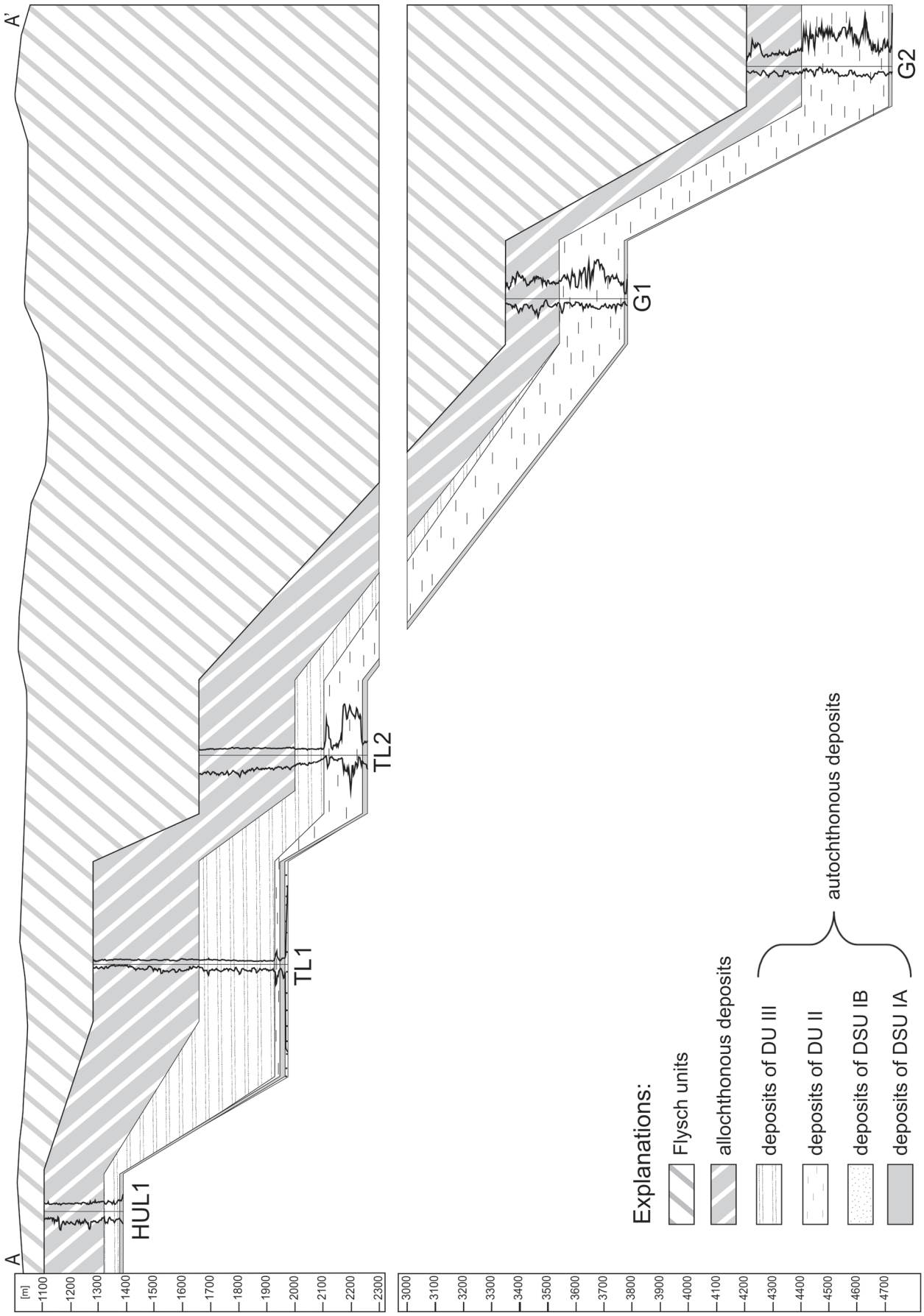

Fig. 5A. Representative log cross-section situated in SE–NW direction, in line of paleovalley.

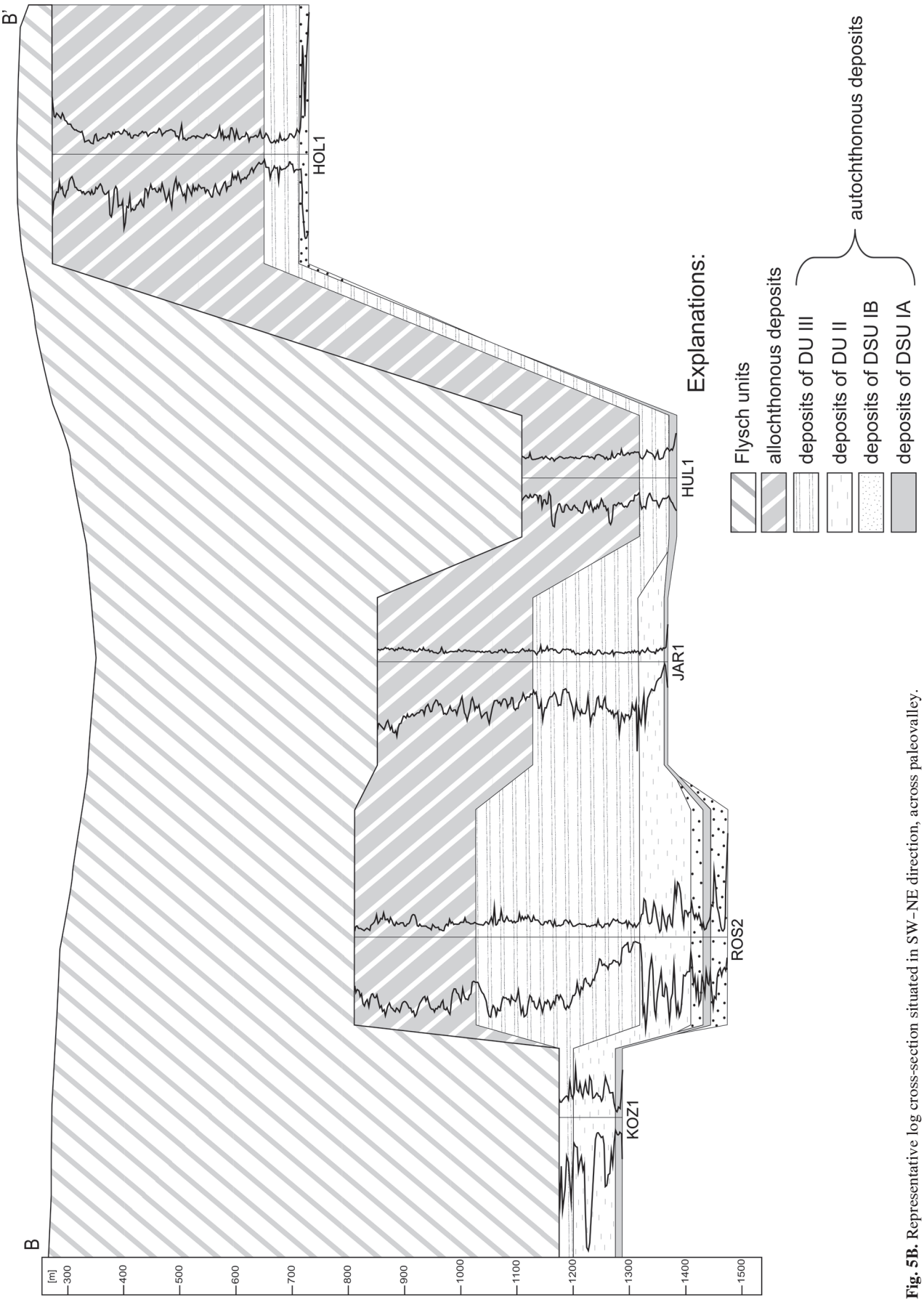

Fig. 5B. Representative log cross-section situated in SW–NE direction, across paleovalley.

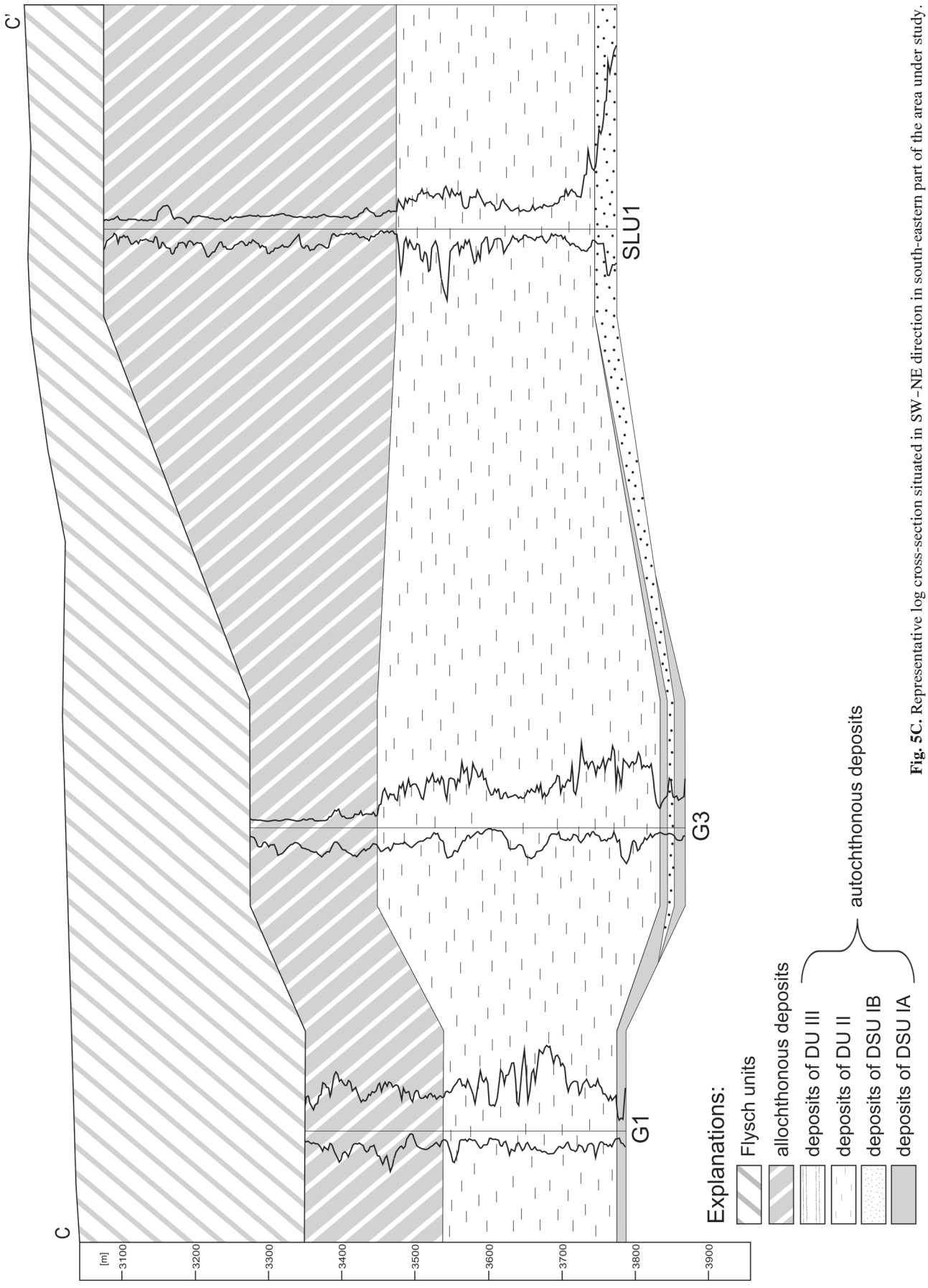

Fig. 5C. Representative log cross-section situated in SW–NE direction in south-eastern part of the area under study.

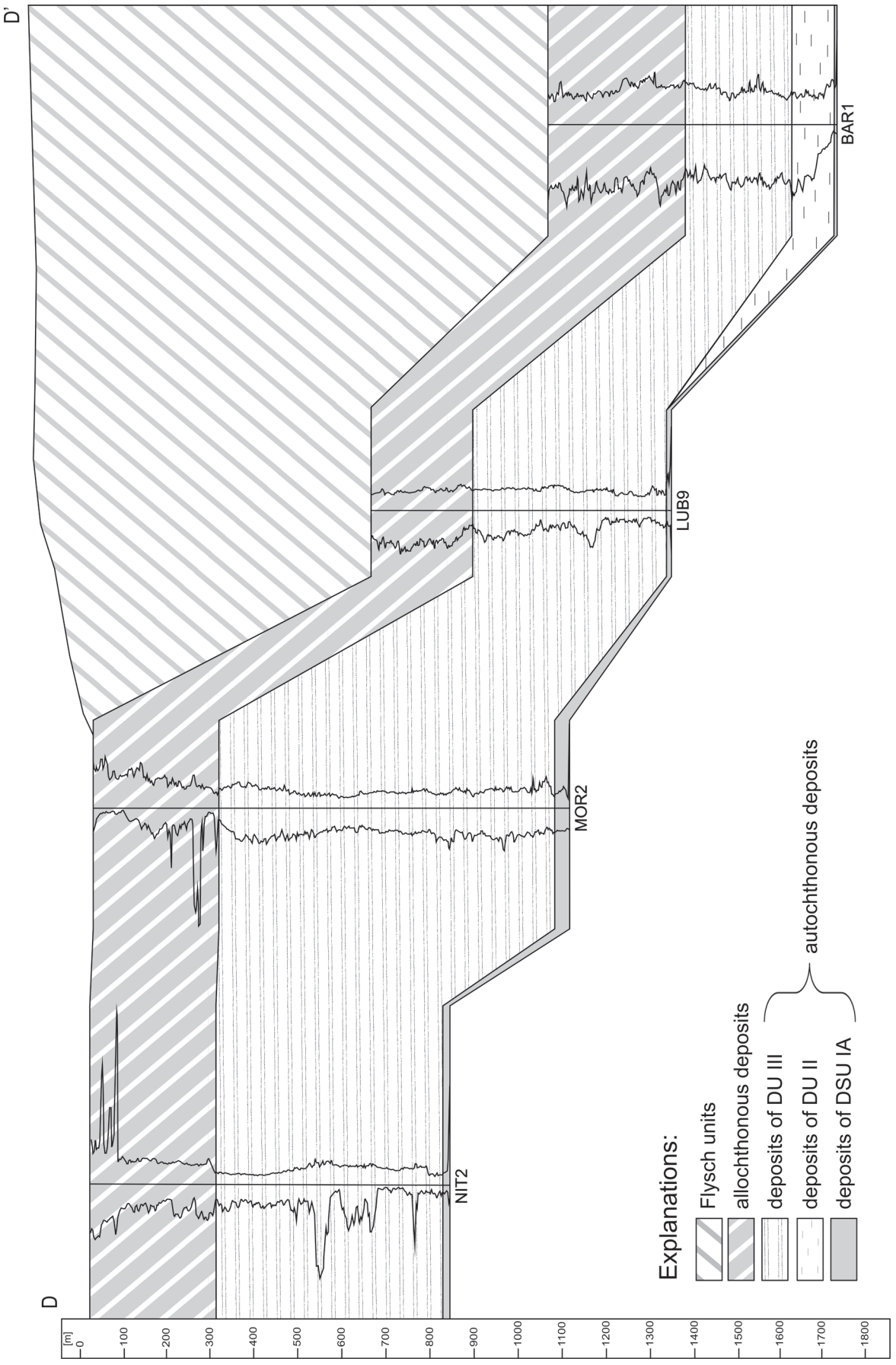

Fig. 5D. Representative log cross-section situated in W–E direction in south-western part area under study.

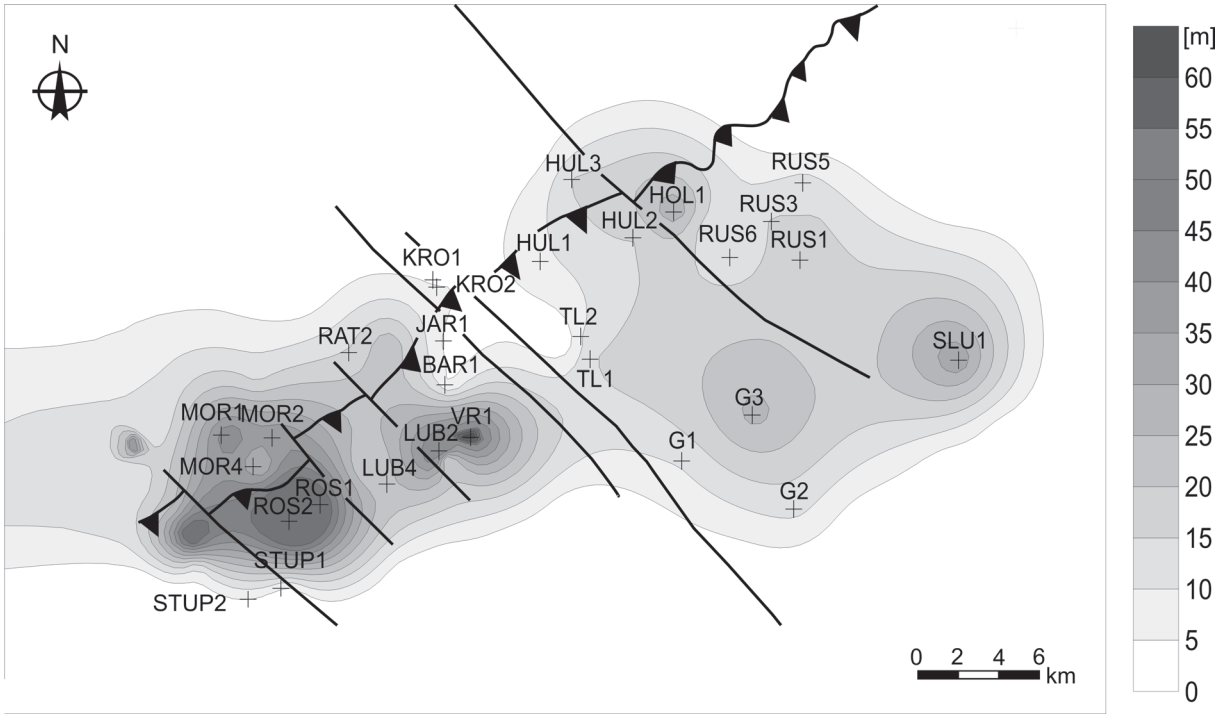

Fig. 6. Thickness map of the depositional unit I.

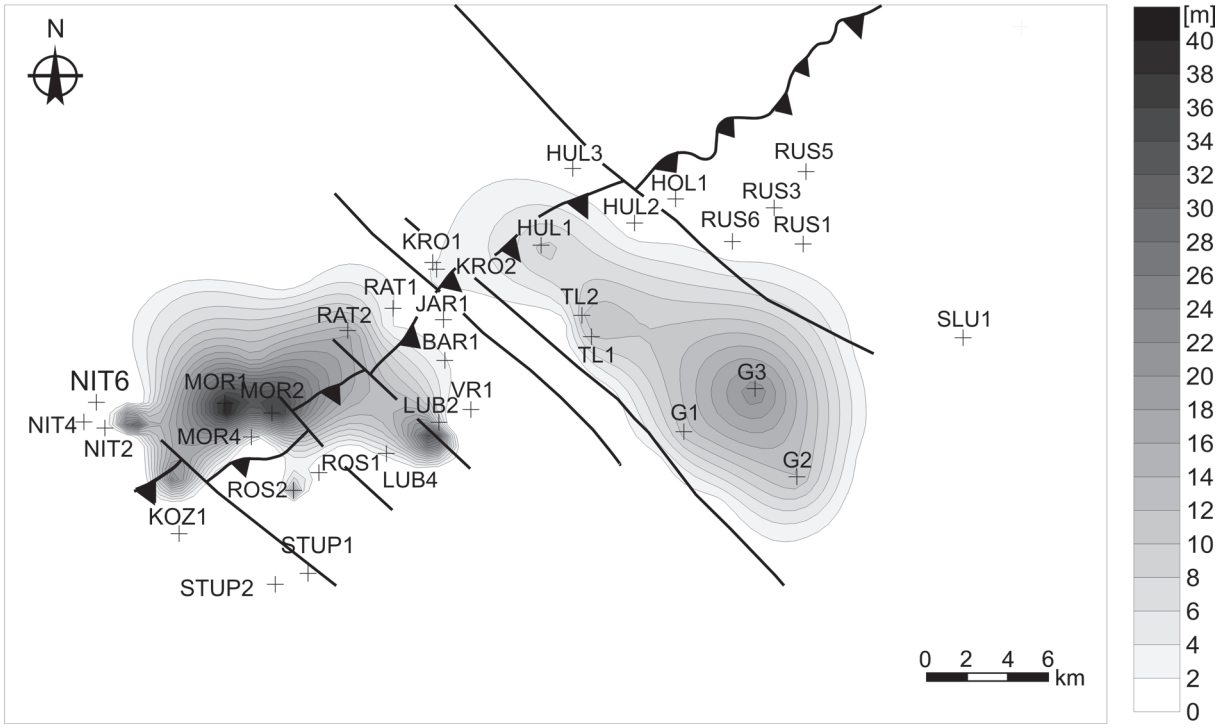

Fig. 7A. Thickness map of the depositional subunit IA.

and shelf. Such conditions are also prone to a high variety of shallow marine processes (wave action, tidal processes, storm action, etc.) and environments. Relic and only local preservation of facies G compared to sandstone facies within the subunit IB points to localized positions of the steeper and shorter coast (Wright et al. 1979). Preservation of the depositional subunit IB can reflect a "stepped transgression" (Bergman & Walker 1988; Walker & Plint 1992). The relatively large thickness of subunit IB together with the important role of the foreshore and upper shoreface deposits points to a high-energy coast (Clifton 1976; Galloway & Hobday 1996), but a possible amalgamation to DU II cannot be excluded.

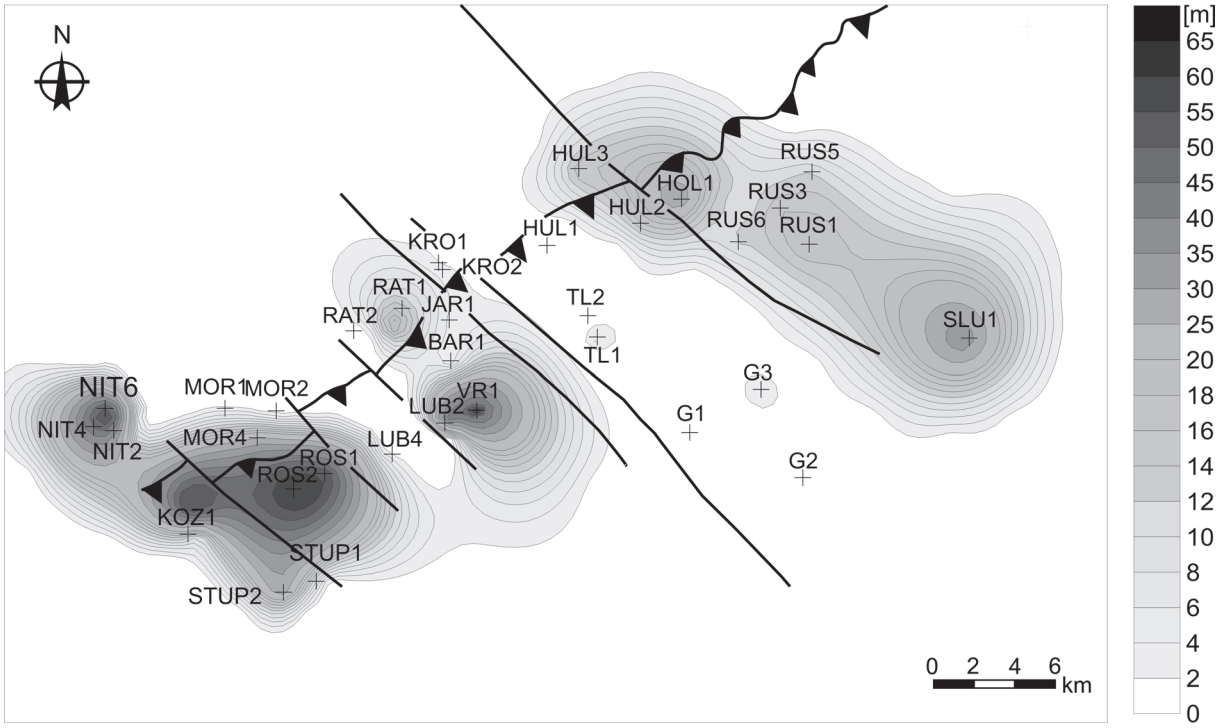

Fig. 7B. Thickness map of the depositional subunit IB.

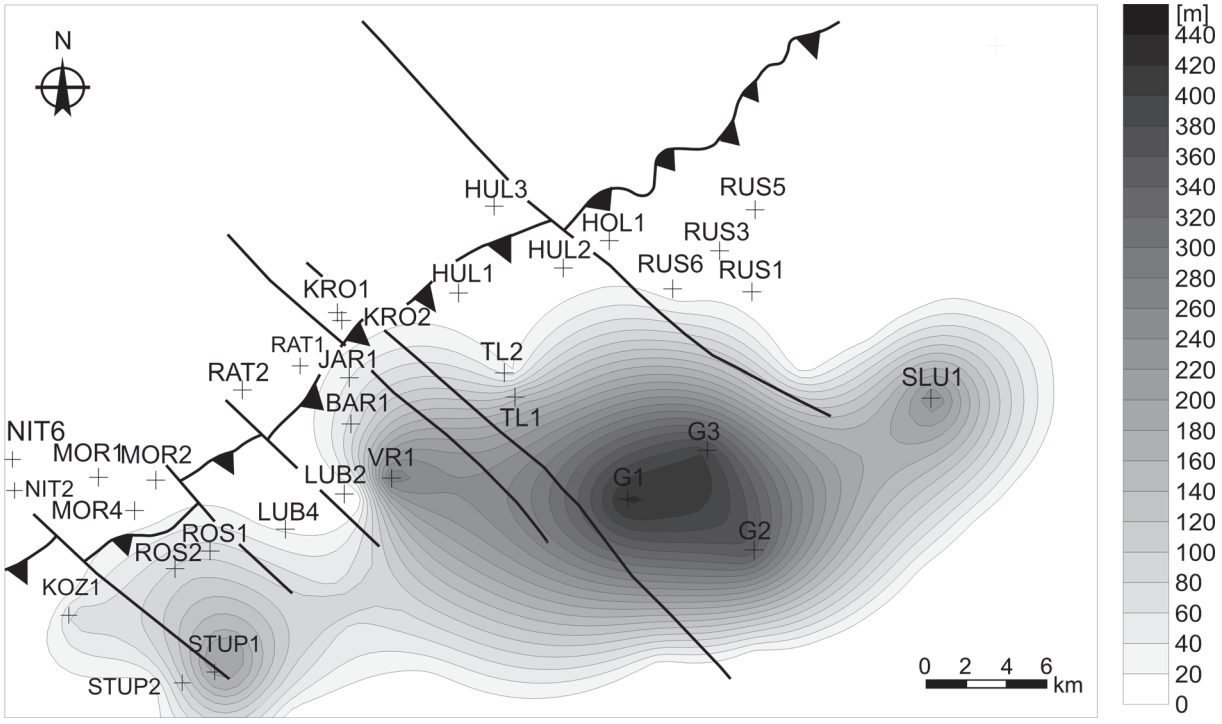

Fig. 8. Thickness map of the depositional unit II.

The deposits of the DU II can be compared to the Mušov Mb. (Adámek et al. 2003) and are faunistically characterized by globigerinas and *Uvigerina bononiensis* (Thonová et al. 1987). The basal contact of DU II and subunit IB represents a significant lithological boundary, which is interpreted as a lower shoreface/offshore boundary. Such a boundary is commonly located at depths of 40 to 90 m (see Drake & Cacchione 1985; Nittrouer et al. 1986). Recognized coarsening-upward cycles are interpreted as parasequences and their repetition points to a deeper intervention of sand into the shallow marine condition. Facies analysis reveals a significant role of storms, which are probably mostly responsible

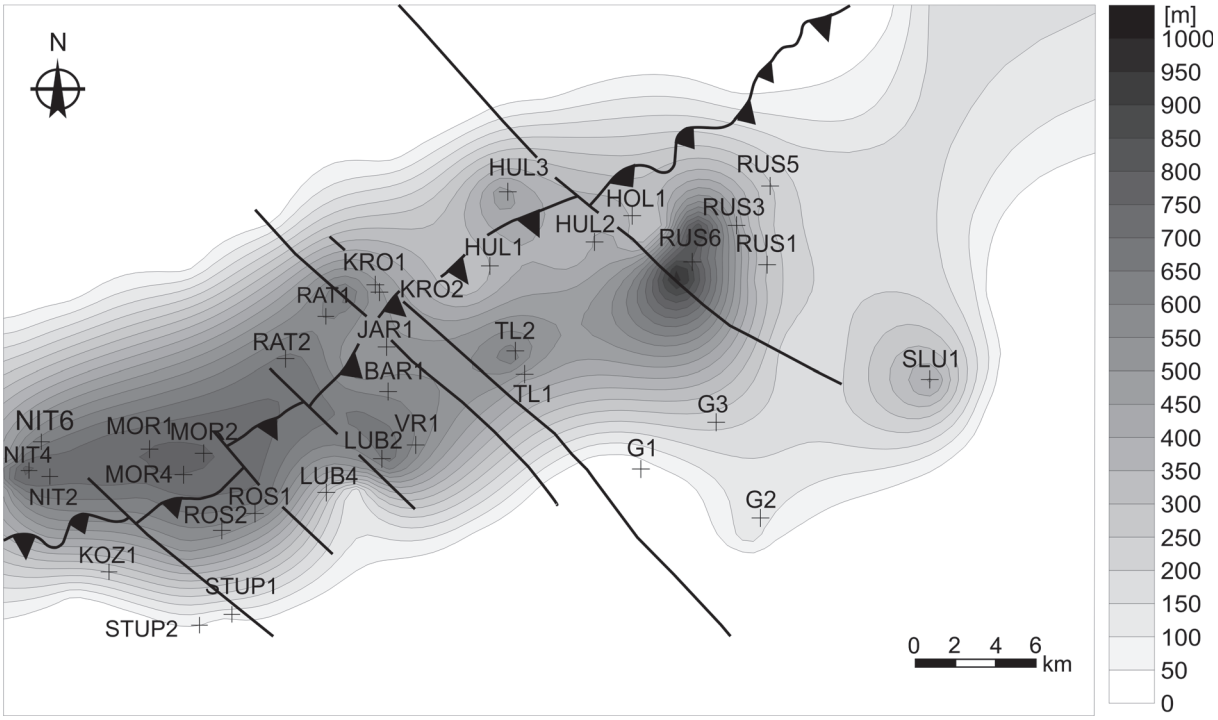

Fig. 9. Thickness map of the depositional unit III.

for offshore sand delivery. The DU II is mostly interpreted as a retrograding parasequence set, when general transgressive trends and shifts of the shoreline to the foreland are interrupted by short-term regressions (undulating "zig-zag" shoreline trajectory, Helland-Hansen & Gjelbeg 1994). Continuous shoreline migration led to the enlargement of the shallow marine belt and a "gradual" reduction of the sediment input into the basin, sediment reworking, and redeposition. We can partly speculate about "expanded backstepping parasequences" (Swift et al. 1991), which point to greater formation of accommodation space than sediment delivery.

Significant variations in the thickness of parasequences and parasequence sets were recognized in the central part of the proposed paleovalley compared to its marginal parts (similarly see Dalrymple et al. 1992; Zaitlin et al. 1994), and, similarly, differences in the thickness of the sandy beds were recognized. Although variations in the shoreline trajectory could reflect variations in sediment delivery, they most probably reflect variation in the basement relief, slope, and character of the underlying rocks in the area under study. A relatively slow shoreline retreat with a large role of wave erosion and sediment reworking and so thicker and less extended transgressive deposits could be expected in the areas with higher shoreline slope. However in the flat area, very rapid shoreline retreat and thinner and more extended transgressive deposits can be supposed. Local structural elevation could also serve as the source for the material in the basin and further affect the lateral variability of the transgressive deposits.

The sedimentary infill of the DU III corresponds to the Nový Přerov Mb. with almost faunistically sterile deposits, where individual specimens of *Haplophragmoides cf. vasiceki* were described (Thonová et al. 1987). The DU III represents the shallow marine deposits of the inner shelf, where relatively quiet deposition was rarely disrupted by storm activity (similarly Dott & Bourgeois 1982; Duke 1985). The great thickness and monotonous character of deposits point to an aggrading stacking pattern with a large and balanced formation of accommodation space and sediment delivery. However, both the shape and the thickness of the DU III were probably significantly affected by later thrusting. Occurrence of both deformed and undeformed deposits of the DU III confirmed that the unit is partly composed of duplicated sediment packages formed by deformation or entrainment of pre-existing basin sediments during the thrusting.

Provenance analyses

A wide spectrum of methods of provenance analysis (petrography of sandstones, heavy mineral assemblages, chemistry of garnet, rutile, major and trace elements) has been used for better determination of source area and its evolution.

Petrography of sandstones

The studied sandstones are in general very fine- to medium-grained. The sandy grains have angular and sub-angular shapes. The sandstones are moderately sorted and contain a large amount of monomineral quartz. Aggregate quartz was detected less frequently. The subhedral grains of K-feldspars and plagioclases represent the common component and probably originated from cataclased granitoids. The content

of micas (both biotite and muscovite) varied slightly and they were probably derived from mylonites or cataclased granitoids. Clasts of gneisses, granulites, and feldspar phenocrysts were also identified. Accessory minerals are represented by garnet, zircon, and rutile. The presence of authigenic glauconite was common. Matrix is mainly of the coating type. Cement is formed by carbonates and Fe oxyhydroxides.

The samples of the DU II are predominantly spread within the arkoses field, whereas the samples of the DU III are situated in the wacke field (Fig. 10A — Petránek 1963; Kukal 1986). Some differences in the provenance of sandstones of the DU II and the DU III are also detected from the results of the discrimination diagram Qm–F–Lt (Fig. 10B — Dickinson & Suczek 1979; Dickinson 1985). While the majority of the samples from the DU III occupies the recycled orogen field, the samples from the DU II are more widespread and are located in the magmatic arc fields. Although in the Q–F–L diagram (Fig. 10C — Dickinson & Suczek 1979; Dickinson 1985) the samples from both the DU II and the DU III fall into the recycled field, the samples from the DU II reveal a closer relation to the magmatic arc fields.

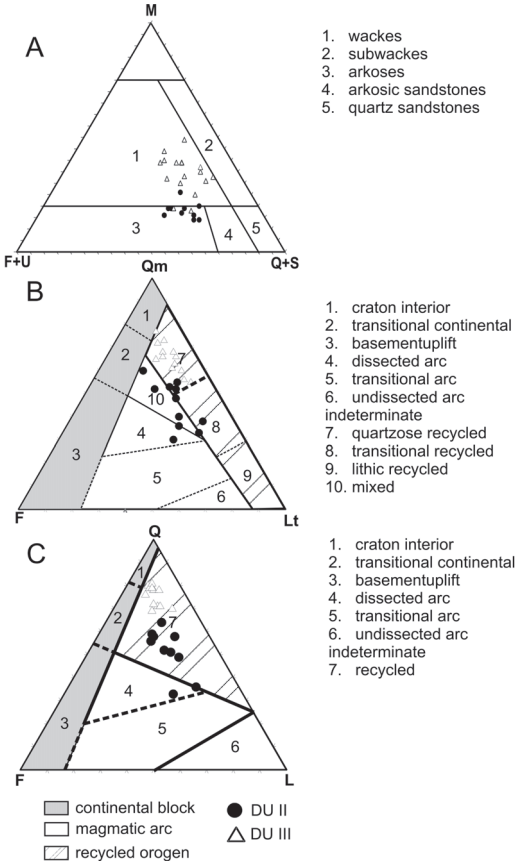

Fig. 10. A — Classification ternary diagram (according to Petránek 1963; Kukal 1986) of the studied sandstones. **M** = matrix (%), **F** = plagioclase + K-feldspar (%), **U** = unstable rock fragments (%), **Q** = quartz (%), **S** = stable rock fragments (%). **B, C** — Discrimination ternary diagrams (according to Dickinson 1985) of the studied sandstones. (**Q** = Q_m + Q_p, **Q_m** — monocrystalline quartz, **Q_p** — polycrystalline quartz; **F** = plagioclase + K-feldspar; **L** = L_v + L_s + L_m, **L_v** — volcanic lithic fragments, **L_s** — sedimentary lithic fragments, **L_m** — metamorphic lithic fragments; **L_t** = L + Q_p).

Studies of heavy minerals

Heavy minerals associations

The dominance of garnet is typical for the heavy minerals association of the studied deposits. Garnet occurrence ranges between 27.1 and 95.4 % (average/AVG 70.4 %). Further commonly identified heavy minerals were apatite (0.9–40.3 %, AVG 10 %), zircon (1.2–24.8 %, AVG 4.5 %), tourmaline (5.1–22.1 %, AVG 4.5 %), and rutile (0.7–41.3 %, AVG 6.2 %). The occurrence of kyanite, sillimanite, staurolite, monazite, anatase, titanite, epidote, amphibole, and pyroxene varies greatly and reaches a maximum of 1 %. The value of the ZTR (zircon+tourmaline+rutile index — Hubert 1962; Morton & Hallsworth 1994) varies greatly, ranging between 8.4 and 64.9 (AVG 12.3 %). Any significant trends were recognized in the heavy mineral assemblages or value of the ZTR index within the studied succession.

The important occurrence of ultrastable heavy minerals is generally typical for deeply buried deposits and can be expressed by the garnet/zircon (GZi) index (Morton & Hallsworth 1994; 1999). According to Morton (1984), garnets underwent dissolution when buried at depths exceeding 3 km. Milliken (1988) placed this dissolution at a depth of 4 km. However, the average values of the GZi index for G 2 (samples from depths of 4297–4484 m) and Slu 1 (samples from depths of 3203–3697 m) vary between 88 and 95 %, which do not indicate such a burial effect.

Garnet

Garnet, as the most common heavy mineral, was further evaluated by analysis of its chemistry, which is widely used for the determination of provenance (Morton 1991; Morton et al. 2004; Salata 2004, 2013a; b; Nehyba et al. 2012; Suggate & Hall 2013). The composition of garnets was diverse, and 10 garnet types (T1–T10) were determined. T1 is composed of almandine garnets with low contents of pyrope, grossular, and spessartine components and the usual composition is in the range of $Alm_{76-93}Prp_{5-9}Grs_{0-9}Sps_{0-7}$. T2 consists of pyrope-almandine garnets with the composition $Alm_{67-86}Prp_{11-19}Grs_{0-9}Sps_{2-8}$. T3 is composed of pyrope-almandine garnets with an enriched pyrope component and the typical composition is in the range of $Alm_{45-77}Prp_{21-46}Grs_{0-6}Sps_{0-3}$. T4 is represented by grossular-almandine garnets with a composition in the range of $Alm_{59-78}Grs_{11-20}Prp_{6-9}Sps_{1-7}$. T5 consists of grossular-almandine garnets with increased content of grossular and the composition $Alm_{53-68}Grs_{21-32}Prp_{5-9}Sps_{1-9}$. T6 is represented by pyrope-almandine garnets with increased contents of grossular and the composition $Alm_{55-75}Prp_{12-27}Grs_{11-18}Sps_{0-3}$. T7 is formed by grossular-almandine garnets with increased contents of pyrope and the composition $Alm_{40-76}Grs_{12-28}Prp_{11-26}Sps_{1-6}$. T8 consists of spessartine-almandine garnets and a composition in the range of $Alm_{47-72}Sps_{11-38}Prp_{3-9}Grs_{0-9}$. T9 is composed of almandine-spessartine garnets with the composition

$Sps_{46-53}Alm_{31-36}Prp_{5-10}Grs_{0-5}$. Lastly, T10 is represented by garnets with varied compositions and individual occurrences. The representatives of this group are $Sps_{41-45}Alm_{36-39}Prp_{13-16}$ (3 grains), $Alm_{55-61}Grs_{17-18}Sps_{11-15}$ (3 grains), $Alm_{37-59}Sps_{17-37}Grs_{13}$ (3 grains) $Sps_{50}Alm_{32}Grs_{12}$, $Grs_{40}Sps_{28}Alm_{24}$, $Grs_{46}Alm_{36}Sps_{14}$, and $Prp_{49}Alm_{31}Grs_{18}$ (one grain). Table 2 shows the relative abundance of these garnet types in the studied samples.

The distribution of recognized garnet types T1–10 varies within the identified DU. The subunit IB is characterized by dominance of T1 (20.3 %), T4 (16.9 %), and T2 (15.3 %). The most comon garnets in the DU II are T1 (25.8 %), T4 (21.1 %), and T2 (18.3 %). The DU III is characterized by T2 (22.5 %), T4 (17.8 %), and T3 (14.6 %). The subunit IB is characterized by a significantly higher proportion (10.2 %) of spessartine-almandine garnets (T8) compared to the DU II (3.3 %) and the DU III (4.2 %). The detrital garnet assemblages of the DU II contain significantly higher number of (25.8 %) of almandine garnets (T1) than the DU III (8.0 %). The representation of specific types of garnets in the individual DU is illustrated in Fig. 11.

The composition of the garnets of the studied Karpatian deposits could be compared with the results of garnet analyses from some potential source rocks, that is, the underlying crystalline rocks of the Brunovistulicum, sandstones and greywackes of the Moravo-Silesian Paleozoic deposits (Drahany and Nízký Jeseník Culmian facies), sandstones of the Magura Group (Rača Unit), sandstones of the Krosno-Menilite Group (Silesian Unit), and older Eggenburgian-Ottnangian infill of the Carpathian Foredeep Basin.

The pyrope-almandine-spessartine and pyrope-spessartine-almandine garnets with compositions in the range of $Sps_{39-47}Alm_{35-42}Prp_{13-16}Grs_{0-4}$ and $Alm_{38-46}Sps_{35-40}Prp_{13-15}Grs_{0-2}$ are typical of the underlying crystalline rocks.

The detrital garnets of the older parts of the Moravian-Silesian Paleozoic deposits (Protivanov and the lower part of the Myslejovice Formation) are clustered in the field of spessartine in the ternary diagram Grs–Prp–Sps (Fig. 12A). The upper part of the Myslejovice Formation contains predominantly pyrope-almandine garnets (Otava et al. 2000; Čopjaková et al. 2002; 2005; Čopjaková 2007) clustered in the field of pyrope (see Fig. 12B).

The pyrope-almandine garnets dominate in the Rača Unit (Otava et al. 1997; 1998) with a trend of Prp–Sps in the ternary diagram Grs–Prp–Sps (see Fig. 12C). The pyrope-almandine and grossular–almandine garnets predominate in the Silesian Unit (Stráník et al. 2007) and form a linear trend Prp–Grs in the ternary diagram Grs–Prp–Sps (see Fig. 12D).

Similarly, the pyrope-almandines are the predominant garnets of the Eggenburgian and Ottnangian deposits (Nehyba & Buriánek 2004).

Rutile

The concentration of the main diagnostic elements of rutile (Fe, Nb, Cr, and Zr) varies significantly in the studied samples. The concentration of Fe ranges between 450 and 9390 ppm (average 3184 ppm), the concentration of Nb ranges between 70 and 9630 ppm (average 2636 ppm), the concentration of Cr ranges between 0 and 2680 ppm (average 643 ppm), and the concentration of Zr varies between 20 and 5390 ppm (average 438 ppm).

The content of Fe is used an as indicator to distinguish the igneous and metamorphic origin of rutiles (Zack et al. 2004a; b). Provenance from igneous rocks was very minor and such rutiles represent about 9.7 % of the studied spectra. The absolute majority of the investigated rutiles originated from metamorphic rocks. Rutiles derived from metapelitic rocks dominate in the DU III (87.5 %) over rutiles from metamafites (12.5 %). Similarly, in the DU II metapelitic (75.6 %) rutile predominates over metamafic (24.4 %) ones (see Fig. 13). The rutiles from the DU III (47 grains) reveal higher contents of Nb and Cr compared to the rutiles from the DU II (43 grains). It is supposed that felsic granulites and paragneisses dominate and garnet amphibolites, and eclogites have a subordinate role in the source area (see Meinhold et al. 2008). The contents of Zr in rutile can be used as a thermometer (Zack et al. 2004a; Watson et al. 2006; Meinhold et al. 2008; Meinhold 2010). The calculated temperatures range between 372–1088 °C (equation Zack et al. 2004) and 464–958 °C (equation Watson et al. 2006) respectively (Fig. 14). The Figure 15 shows the possible relative abundance of different metamorphic facies in the source area of the studied deposits with dominance of medium- to high-temperature amphibolite/eclogite facies.

Table 2: Garnet types of the studied deposits (**Alm** — almandine, **Grs** — grossular, **Prp** — pyrope, **Sps** — spessartine).

	DEPOSITIONAL SUBUNIT IB [51 grains]	DEPOSITIONAL UNIT II [126 grains]	DEPOSITIONAL UNIT III [159 grains]
Alm_{76-93}	20.3%	25.8%	8.0%
$Alm_{67-86}Prp_{11-19}$	15.3%	18.3%	22.5%
$Alm_{45-77}Prp_{21-46}$	13.6%	6.6%	14.6%
$Alm_{59-78}Grs_{11-20}$	16.9%	21.1%	17.8%
$Alm_{53-68}Grs_{21-32}$	3.4%	4.2%	11.3%
$Alm_{55-75}Prp_{12-27}Grs_{11-18}$	6.8%	5.2%	6.1%
$Alm_{40-76}Grs_{12-28}Prp_{11-26}$	5.1%	12.2%	10.3%
$Alm_{41-72}Sps_{11-42}$	10.2%	3.3%	4.2%
$Sps_{46-53}Alm_{31-36}$	3.4%	1.4%	–
$Sps_{41-45}Alm_{36-39}Prp_{13-16}$	–	–	1.4%
$Alm_{55-61}Grs_{17-18}Sps_{11-15}$	3.4%	0.5%	0.9%
$Alm_{37-59}Sps_{17-37}Grs_{13}$	1.6%	1.4%	0.9%
$Sps_{50}Alm_{32}Grs_{12}$	–	–	0.5%
$Grs_{40}Sps_{28}Alm_{24}$	–	–	0.5%
$Grs_{46}Alm_{36}Sps_{14}$	–	–	0.5%
$Prp_{49}Alm_{31}Grs_{18}$	–	–	0.5%

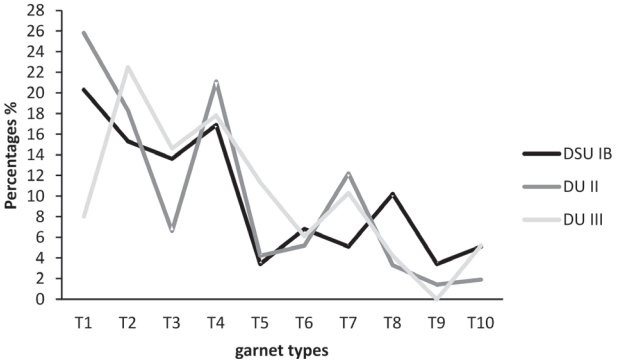

Fig. 11. Distribution plot of the recognized garnet types.

The temperatures were calculated for 40 grains of rutile where Zr was detected.

Major element geochemistry

The major element composition is presented in Appendix 1*. The TiO_2 content is relatively low and stable in the studied samples, whereas the Al_2O_3 content is significantly more variable. The Al_2O_3 versus TiO_2 diagram (Nesbitt & Young 1998; Andersson et al. 2004) is presented in Fig. 16A. A relatively low content of TiO_2 and high content of Al_2O_3 was recognized for the DU I. Two clusters according to sample grain size can be followed for the DU II. Relatively low contents of both Al_2O_3 and TiO_2 are typical for the first

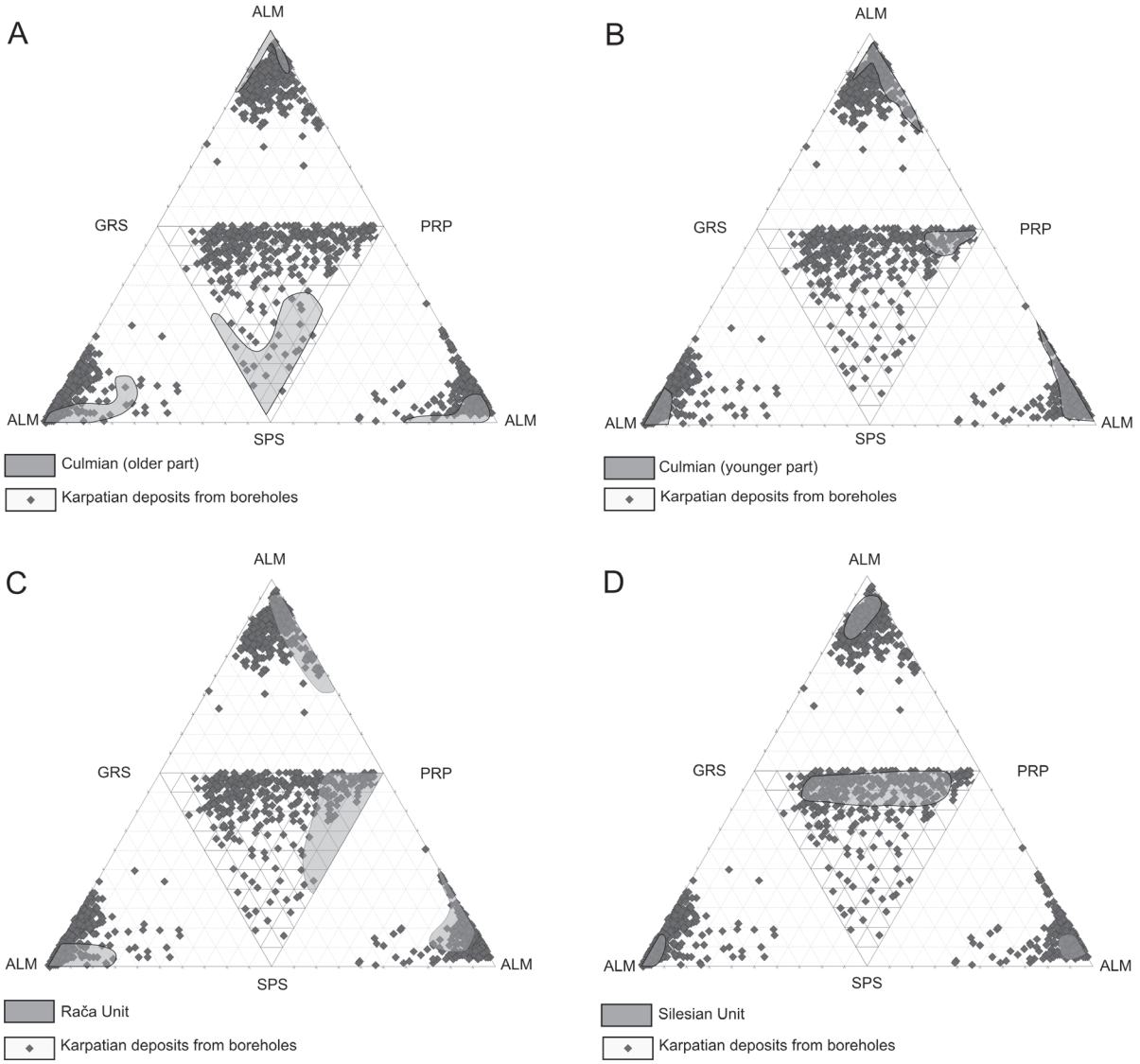

Fig. 12. Ternary diagram of the chemistry of the detrital garnets. **A** — comparison with the chemistry of detrital garnets from older part of Moravian-Silesian Paleozoic (Culmian) (Otava et al. 2000; Čopjaková et al. 2002; 2005; Čopjaková 2007). **B** — comparison with the chemistry of detrital garnets from younger part of Moravian-Silesian Paleozoic (Culmian) (Otava et al. 2000; Čopjaková et al. 2002; 2005; Čopjaková 2007). **C** — comparison with the chemistry of detrital garnets from Rača Unit (Otava et al. 1997; 1998). **D** — comparison with the chemistry of detrital garnets from Silesian Unit (Stráník et al. 2007). (**ALM** – almandine, **GRS** – grossular, **PRP** – pyrope, **SPS** – spessartine).

* Appendix-1 — only in an electronical version on *www.geologicacarpathica.com*

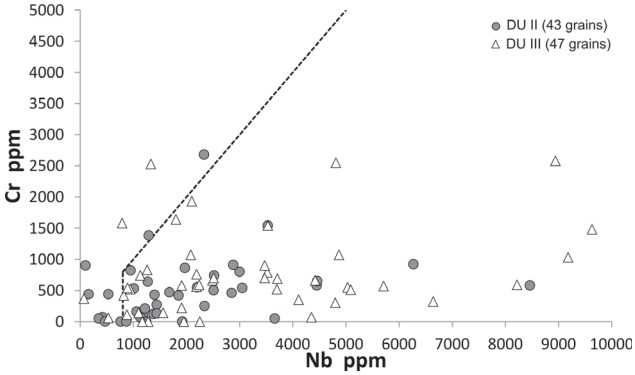

Fig. 13. Discrimination plot Cr vs. Nb of investigated rutiles (according to Meinhold et al. 2008).

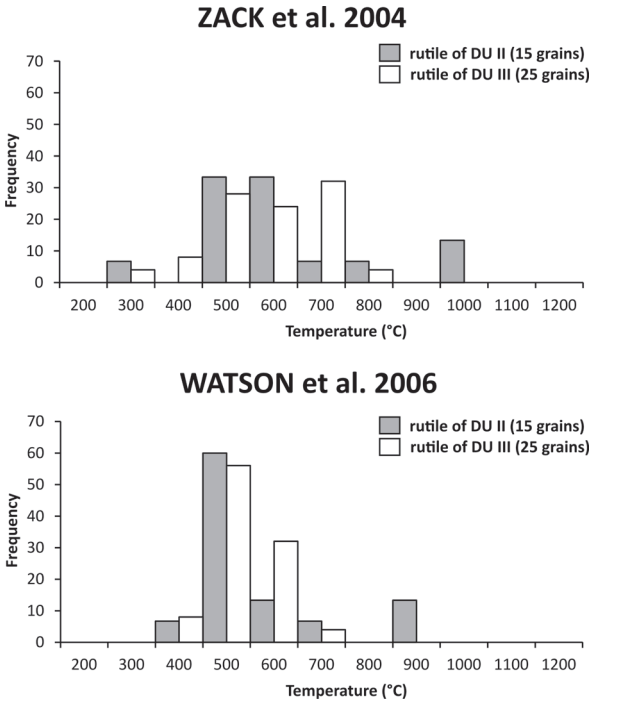

Fig. 14. Histogram of calculated temperatures for rutiles from DU II and DU III. Temperatures were calculated based on the equation of Zack et al. (2004a) and equation of Watson et al. (2006).

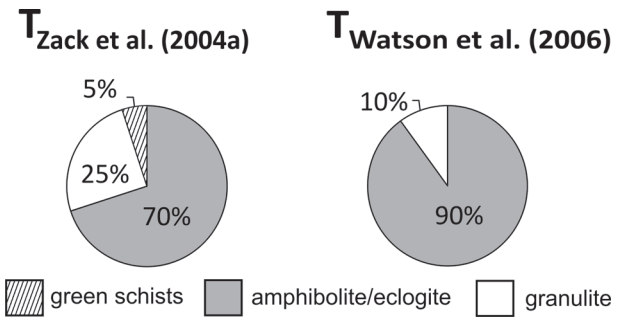

Fig. 15. Diagrams showing the percentage of the different metamorphic facies for the source rocks according to calculated temperatures.

cluster (sandstones), whereas higher values of Al_2O_3 and TiO_2 are typical for the second one (mudstones). While positive correlation of Al_2O_3 and TiO_2 is typical for the data from the DU I and the DU II, the results for the DU III shows significant differences in the Al_2O_3 content and a relatively stable content of TiO_2. Such a horizontal distribution reflects the different weathering and sorting of the sand fraction.

The TiO_2/Zr versus Zr/Al_2O_3 diagram (Fig. 16B) reveals an almost linear distribution and negative correlation. Generally similar arrangements for results from individual depositional units can be followed in this diagram as in the Al_2O_3 versus TiO_2 diagram.

Distinct trends in the Al_2O_3 versus TiO_2 and TiO_2/Zr versus Zr/Al_2O_3 diagrams are significantly influenced by grain-size sorting. The main TiO_2 origin probably come from minerals such as biotite, amphibole, and pyroxene or olivine (Nesbitt 1979; Taylor & McLennan 1985). The low Al_2O_3 and TiO_2 contents of the studied deposits could point to a source from granulites and granitoids (Passchier & Whitehead 2006), and the position of all samples in an almost curvilinear line suggests a uniform/similar source (Fralick & Kronberg 1997; Passchier & Whitehead 2006).

The studied samples are sedimentary rocks from heterogeneous source rocks which might have undergone different weathering processes and intensities. The values of CIA range from 56.84 to 80.89 for the studied samples. The CIA of sediments is, in general, about 50 in the case of first cycle sediments and tends to increase as chemical weathering intensifies (Nesbitt & Young 1982). The obtained values correspond to intermediate chemical weathering and an important source from recycled material (Fedo et al. 1995). The variations in CIA reflect differences in the proportion of the content of weathered/recycled material. The data were plotted in the A–CN–K (Al_2O_3–(CaO+Na_2O)–K_2O diagram (Fig. 16C). All the studied samples are distributed parallel to the A–CN axis and follow a trend of increasing Al_2O_3 with decreasing CaO+Na_2O. The elongated distribution reflects the varied role of the weathering trend/clay minerals and can be associated with grain-size variations (Corcoran 2005). The A–CN–K triangle is also used to determine the composition of the parent rocks (Fedo et al. 1995) and the results indicate a similar source.

SiO_2/Al_2O_3 is known as the index of chemical maturity of sediments (Roser et al. 1996; Roser & Korsch 1999). The SiO_2/Al_2O_3 ratio ranges from 2.54 to 13.82 (AVG 5.10). According to Zhang (2004), the low SiO_2/Al_2O_3 ratios indicate a low sediment recycling and deposition from a nearby source. Negative correlation between SiO_2 and Al_2O_3 for the studied samples can be followed in the Fig. 16D and is a result of the varied presence of mud material. A similar distribution of samples in Fig. 16A–E points to the principal role of grain size (Ross & Bustin 2009; Adegoke et al. 2014).

The degree of chemical maturity of sediments is also expressed by the diagram of Al_2O_3+K_2O+Na_2O versus SiO_2 (Suttner & Dutta 1986; Sen et al. 2012). The studied samples have values of chemical maturity in the range from 0.10 to 0.51 (AVG 0.3). The results in the arid field are derived from mudstones while the results in the humid field are derived from sandstones (Fig. 16E).

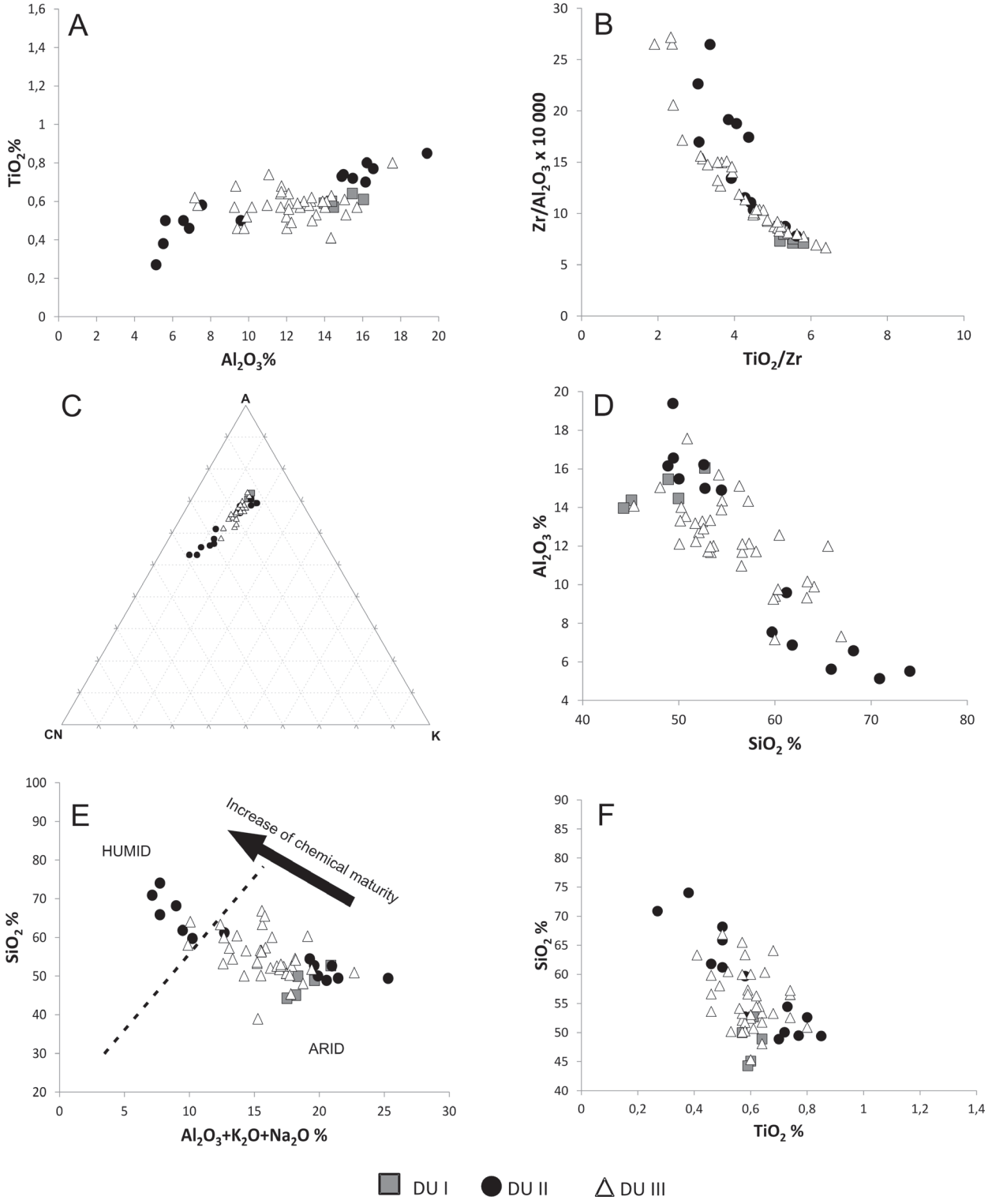

Fig. 16. Discrimination plots of major element geochemistry. **A** — TiO_2 vs. Al_2O_3, **B** — TiO_2/Zr vs. Zr/Al_2O_3, **C** — ternary diagram Al_2O_3–$(CaO+Na_2O)$–K_2O, **D** — Al_2O_3 vs. SiO_2, **E** — SiO_2 vs. $Al_2O_3+K_2O+Na_2O$, **F** — SiO_2 vs. TiO_2.

With no extra input of detritus, the sediment recycling results in a negative correlation of SiO_2 and TiO_2 (Gu et al. 2002). Such a trend can generally be followed for the studied samples (Fig. 16F). In the ideal case (Cox & Lowe 1995; Corcoran 2005) the overlying sequence/formation should contain more quartz (i.e. SiO_2) and less feldspar and clays (lower contents of TiO_2, Al_2O_3, and MgO). The studied cases show the increase of the sediment recycling for the succession of the DU, but the results are also influenced by grain-size sorting.

Trace element geochemistry

The trace element composition is presented in Appendix 2*. For the determination of the tectonic setting, the samples were plotted on Th–Zr/10–Sc (Fig. 17A) and La–Th–Sc (Fig. 17B) ternary diagrams (Bhatia & Crook 1986). The samples from all depositional units lie mostly inside the discrimination field of the continental island arc (McLennan et al. 1993; Bahlburg 1998). The results are arranged in a line (Fig. 17A) or a cluster (Fig. 17B) and point to a similar source of the studied deposits. Different maturities of sediments are observable in the ternary diagram Th–Zr/10–Sc. Zr contents in the deposits are increased depending on the maturity of sediments.

Obtained Th/Sc and Zr/Sc values are distributed along the trend from the mantle to upper continental crust compositions (McLennan et al. 1993). A relatively low role of sediment recycling and compositional variations is visible in the plot diagram (Fig. 17C). The samples from the DU I reveal the smallest role of recycling and a relatively uniform source, whereas the role of recycling and source rock heterogeneity is pronounced for the DU III.

The degree of recycling can also be determined using the Zr/Th ratio (Zimmermann & Bahlburg 2003). The studied samples display Zr/Th ratios between 9.30 and 37.79. Such relatively low values indicate the relatively small role of reworking. The lowest values of the Zr/Th ratio are in the DU I; by contrast, the highest ones were recognized for the sandy samples of the DU II.

The values of the Cr/Ni ratios of the studied deposits vary from 1.04 to 2.85 and the sources of the studied deposits correspond to felsic rocks. A diagram of Cr/V and Y/Ni ratios (Fig. 17D) is used for determination of the provenance. The Cr/V ratios are used as an index of the enrichment of Cr over the ferromagnesian trace elements. The Y/Ni ratios monitor the content of ferromagnesian trace elements compared with a proxy for HREE. The ultramafic rocks have higher Cr/V and lower Y/Ni ratios (Hiscott 1984; McLennan et al. 1993;

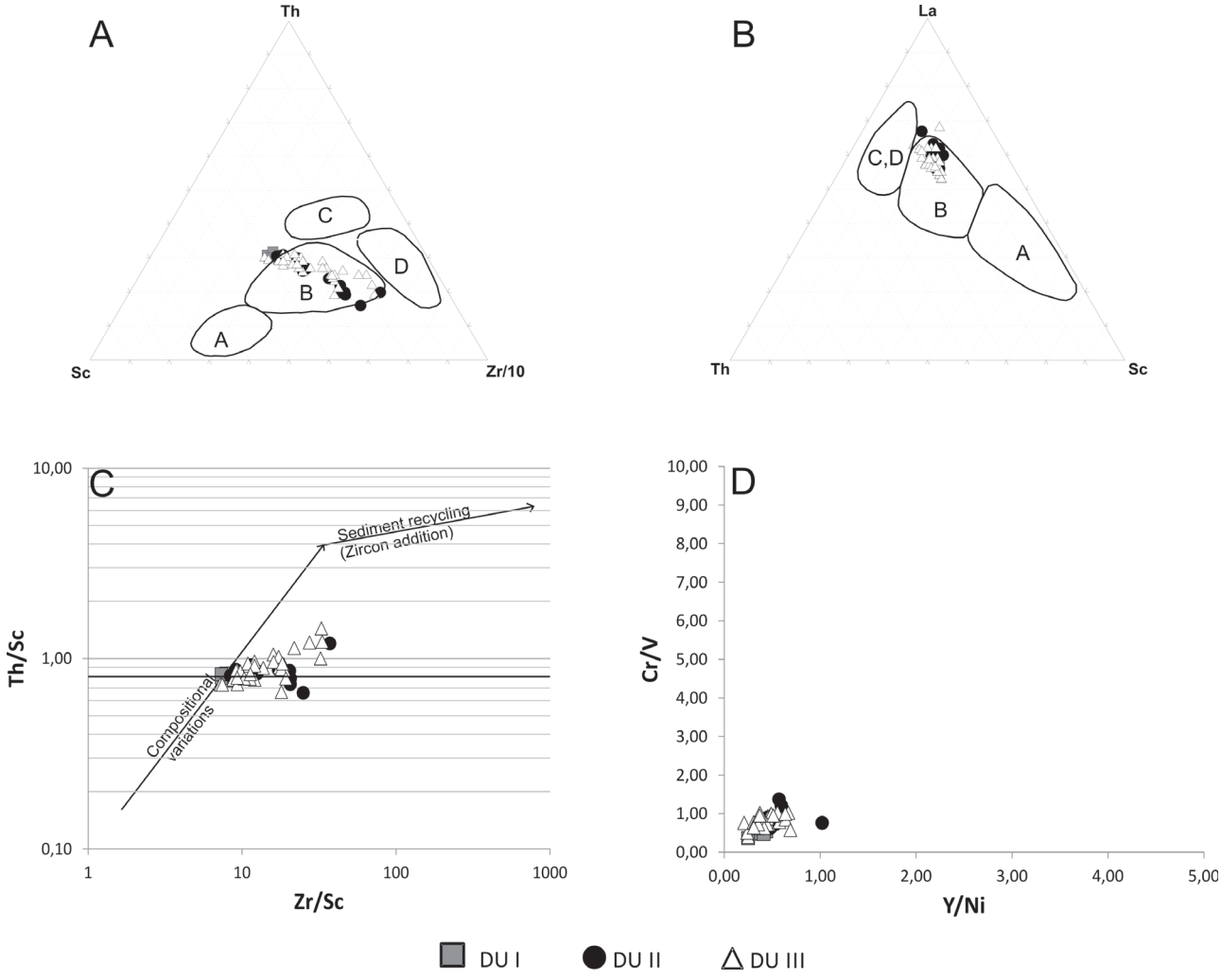

Fig. 17. Discrimination plots of trace element geochemistry. **A** — Th-Zr/10-Sc ternary diagram, **B** — La-Th-Sc ternary diagram; (A) Oceanic Island Arc, (B) Continental Island Arc, (C) Active Continental Margin, (D) Passive Margin, **C** — Th/Sc vs. Zr/Sc, **D** — Cr/V vs. Y/Ni.

* Appendix-2 — only in an electronical version on *www.geologicacarpathica.com*

Ali et al. 2014). The studied samples have an extremely low Cr/V ratio and low Y/Ni ratios, indicating predominantly felsic source rocks.

Interpretation

The poor development of the burial effect on the association of the heavy minerals and garnet chemistry could be explained by the relatively short duration of diagenetic processes. These results signify that the studied heavy minerals associations were dominantly influenced by the composition of the source rocks.

The rutile analyses proved that the primary source was crystalline rocks of the Bohemian Massif (Moldanubian and Moravian Zones). The rocks of the Bohemian Massif were recognized in the Račice and Luleč conglomerates of the Moravo-Silesian Paleozoic deposits (Čopjaková 2007) and these conglomerates are probably supposed to represent the source of the studied deposits.

Although similar heavy mineral associations are known from both the Rača Unit (Gilíková et al. 2002) and Myslejovice Formation (Otava 1998; Čopjaková 2007), the chemistry of garnets discriminates between the sources more precisely.

Occurrence of spessartine-almandine garnets (T8) proved that the crystalline rocks of the local basement can be considered as an important source for the subunit IB. The source of almandine garnets (T1) can be traced well to the Luleč conglomerates (the young part of Myslejovice Formation) (Čopjaková 2007). These garnets are missing in the Rača Unit and the Silesian Unit that contain pyrope-almandine (T2, 3) and grossular-almandine garnets (T4, 5). It can be assumed that the early phases of the sedimentation (DU I and II – the forebulge depozone) were supplied from the passive/foreland margin of the basin, that is, from the Bohemian Massif. The slight differences in provenance between units I and II (the variations in the role of the local crystalline basement and the more distant Moravo-Silesian Paleozoic deposits) can be explained by the basin and source area enlargement.

Both the small content of garnet T1 and the abundance of T3 point to a change of the source area for the later phases of deposition (i.e. the DU III). The significant role of the source from the Silesian Unit (active margin – the Western Carpathian Flych Zone) and its mixing with material from the Bohemian Massif is proposed. This points to shift of the depozones towards the orogenic wedge, that is, to the foredeep depozone.

The cannibalization of the older basin infill (Eggenburgian and Ottnangian deposits) and its role as a partial source for the studied Karpatian deposits cannot be excluded.

The results of garnets are partly supported by petrography (see Fig. 10B).

Discussion

The stacking pattern of facies associations of the Karpatian basin infill in the studied well cores, the temporal and spatial evolution of the depozones, and the results of the provenance analyses can all be summarized and evaluated according to the principles of the sequence stratigraphy and proposed models of peripheral foreland basin evolution (Flemings & Jordan 1990; Jordan & Flemings 1991; Beaumont et al. 1993; Crampton & Allen 1995; DeCelles & Giles 1996). The recognized paleo-environmental changes and paleogeographic evolution of the area point to significant reconstruction of the basin shape and geometry, lateral shifts of the depozones and an important role of basement morphology. A model of the evolution of the basin in the area under study with several depositional stages can be proposed (see Fig. 18):

Stage 1: Increased crustal loading by a thickened orogenic wedge results in subsidence of the inner part of the basin and a coeval uplift of the forebulge (Fig. 18A). The fault reactivation (Holešov faults) facilitated the varied/predisposed creation of an accommodation space in the forebulge depozone. Eastward to southeastward flexural dip of the passive basin margin is supposed, with an irregular, generally SW–NE, prolonged shoreline disturbed by a perpendicular paleovalley oriented in the NW–SE direction (along the basement faults, see Fig. 5A, B) where started sedimentation of the depositional subunit IA (Pre- to Early transgressive deposits). The basin depozones continued towards the E-SE.

The stage corresponds to a major pulse of the Carpathian nappe-pile contraction by the Early Styrian phase of thrusting (Ottnangian–Early Karpatian). The stage can be compared with sequence II of Nehyba & Šikula (2007).

Stage 2: The subsequent major marine transgression drowned the embayed margins of the basin. This transgression can most probably be correlated with the Karpatian TB 2.2. sea-level cycle (Haq et al. 1988; Nehyba & Šikula 2007; Hohenegger et al. 2009; 2014). Basin facies belts had been shifted cratonward (i.e. generally towards the northwest) and the adjacent pre-Neogene basement had been drowned. The position of the shoreline (peripheral bulge depozone) was located in the area under study and is represented by the depositional subunit IB. The lagoonal depositional environment, represented by depositional subunit IA, was developed behind the barred coast. This situation is reflected by the NE–SW distribution of depositional subunit IA deposits northwestward to the depositional subunit IB (see Fig. 7A). The continued cratonward shift of the facies belts led to the transition of the shoreline condition to a shallow marine one (transition of depositional subunit IB to the DU II) with more rapid shift towards the northwest within the paleovalley (Fig. 18B). This situation probably mainly reflects the gradual sea-level rise, although early phases of the forebulge retreat might also play a role (Plint et al., 1993; Lesczyński & Nemec 2014). The interplay between sediment supply, basement relief, eustatic sea-level changes, and tectonics affected the frequent bathymetric changes and shoreline trajectory (dynamic stratigraphy of foredeep peripheral unconformity - see Lesczyński & Nemec 2014).

The Neogene tidalites within the Central Paratethys sedimentary basins are known from the Pannonian Basin (Eggenburgian) (Sztanó & de Boer 1995), the North Alpine Foreland Basin (Ottnangian) (Bieg et al. 2007, 2008),

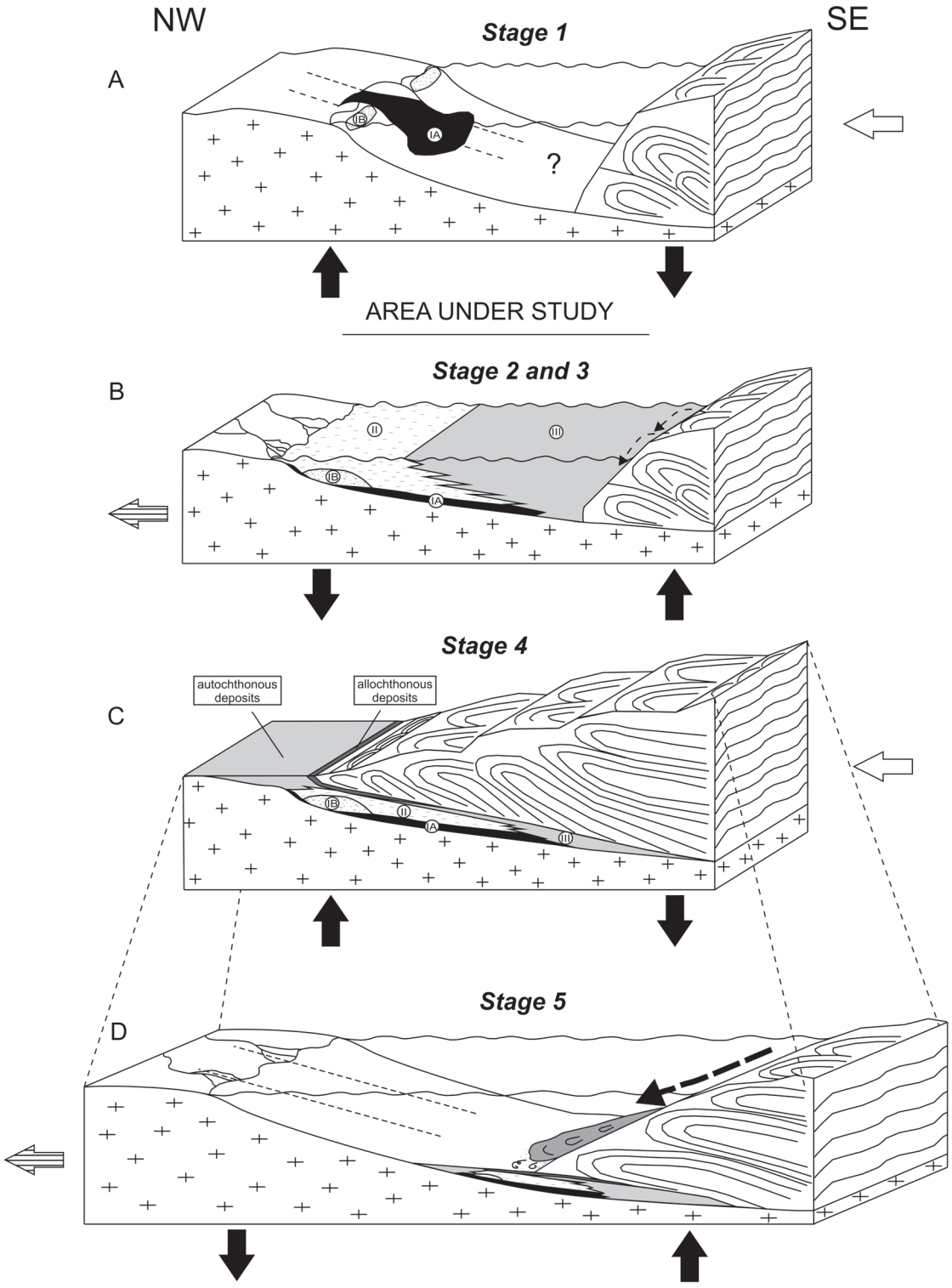

Fig. 18. Schematic evolution of the Carpathian Foredeep. **A** — Increased crustal loading by a thickened orogenic wedge (Carpathian nappes) results in subsidence of the inner part of the foredeep and uplift of the forebulge and sedimentation of DU I. The sediment delivery from passive margin. **B** — The major marine transgression drowned the passive margin and led to the sedimentation of DU II. Decreased crustal loading by orogenic wedge results in cratonward shift of forebulge and sedimentation of DU III. The derivation of the material from both passive and active margin of the basin. **C** — Continued thrusting led to tectonic deformation of the basin infill and shift of the basin subsidence axis northwestward of the area under study. The older basin infill was partly buried under the nappes and the basin geometry was changed. **D** — The deposition in the basin continued outside of the Carpathian thrust front. The basin axis shifted cratonward. Significant sediment delivery from active margin as mass flow deposits (Kroměříž Fm.).

the Korneuburg Basin (Karpatian) (Zuschin et al. 2014), and the Polish and Ukrainian parts of the Carpathian Foredeep (Badenian) (Lis & Wysocka 2012). The tidal flat deposits were not recognized in the sedimentary succession of the Moravian part of the Carpathian Foredeep and their exceptional occurrence is described here only from the spatially restricted area. Such a situation points to an embayed coast. A typical environment for the development of the tidal flat deposits is a tide-dominated estuary (Dalrymple et al. 1992), where its funnel shape tends to increase the tidal current strength (Dalrymple & Choi 2007). The tidal flat deposits probably originated in micro- to meso-tidal conditions.

Stage 3: The rapid forebulge flexural retreat and sediment delivery from the active margin are both reflected by the DU III (Fig. 18B), which was deposited within the foredeep depozone (i.e. the inner part of the foreland basin). The forebulge disconformity/shoreline was rapidly shifted cratonward (northwestward) out of the area under study (Fig. 5A). The position of the coastline/peripheral bulge depozone was probably located more than 50 km northwest. The closest recognized coastline deposits of Karpatian age were documented in the northwest of Prostějov in the borehole Slatinky MH-10 (Bubík & Dvořák 1996). The basin was significantly enlarged and its bathymetry changed. A similar cratonward shift of the foreland basin depozones was described in the North Alpine Foreland Basin in Switzerland, where the forebulge was shifted 100 km towards the northwest (Kempf & Pfiffner 2004). This stage is connected with orogenic quiescence and increased sediment supply from the active margin (Flemings & Jordan 1989; Johnson & Beaumont 1995). Stages 2 and 3 represent the time period between the Early and Late Styrian phases of thrusting and are compared with Sequence III of Nehyba & Šikula (2007).

Stage 4: Renewed loading by orogenic wedge results in subsidence of the inner part of the basin and a coeval uplift of the forebulge. Continuous thrusting led to tectonic deformation of the basin infill and its partial incorporation in the thrust belt in the most proximal/inner part of the basin. Generally westward advance of the nappes led to shift of the lithosphere flexure cratonward and the basin subsidence axis northwestward of the area under study. The inner part of the basin was buried under the nappes or destroyed. Here the original thickness of individual depositional units was tectonically reduced on one side and enlarged on the other (Fig. 18C). The thicknesses of the DU II and the DU III in the studied area are relatively large. These thicknesses are explained by the duplicated sediment packages by so-called overlap of the allochthonous and para-autochthonous Karpatian deposits before the front of nappes. The southeast part of the area under study (around the boreholes G 1, G 2, and G 3) is characterized by complete removal of the DU III and the replacement of the DU II (para-autochthon). The tectonically removed deposits of the DU III were shifted towards the northwest. Benada (1986) recognized the Eggenburgian deposits (Ždánice Unit) between the Karpatian deposits in the borehole Rat 1 and determined the spreading of allochthonous deposits of the Carpathian Foredeep mainly in the northern part of the studied area (boreholes Bar 1, Kro 1, 2, and Rat 1, 2). The basin was limited on its cratonward margin by the uplifted forebulge, which further affected basin extent and bathymetry, so the resulting foreland basin was narrower and deeper. In short, the basin underwent a complete reconstruction of its shape, position, and lateral extent. This stage can be connected with the Late Styrian phase of thrusting (Late Karpatian) and is compared with Sequence IV of Nehyba & Šikula (2007).

Stage 5: The most northwestern part of the area under study belonged to the proximal part of the foreland basin along its active margin. Sediment delivery was from the stacked thrust zone and was highly sensitive to individual tectonic events. This situation is connected with mass flow deposits. The position of the active margin of the basin was probably generally similar to the present state. Further depositional zones of the basin were located more to the W-NW, where they are also preserved (Fig. 18D).

More precise timing of these stages by biostratigraphic data are of little help, because the whole Karpatian is within a single nannoplankton zone NN 4.

Similarly, the inner part of the Polish Carpathians, located beneath the Carpathian nappes, is more than 50 km wide and is composed of Early to Middle Miocene deposits, up to 1500 m thick. However, these Lower Miocene strata are mainly terrestrial in origin (coarse grained alluvial deposits) with a significant portion of material derived from the Carpathian nappes (Oszczypko & Oszczypko-Clowes 2012). Differences in the depositional environments along the basin active margin and in the recognized role of the Carpathian nappes in the provenance (Moravian vs. Polish part of the basin) point to significant variation in the basin geometry, paleobathymetry and sedimentary budget (underfilled stage vs. overfilled conditions).

Conclusions

The Karpatian deposits of the central part of the Carpathian Foredeep in Moravia, are known only from the deep boreholes since they are deeply buried under the Flysch Thrust Wedge of the Outer Western Carpathians. These rocks have been studied by a complex of sedimentological and sedimentary-petrographical methods with the aim of improving our understanding of the paleogeography and evolution of the Carpathian Foredeep basin and reconstructing the former evolutionary stages of this peripheral foreland basin and its paleogeography. The chemistry of detrital garnets has proved to be an important indicator of changes in the provenance of the deposits.

Three depositional units were determined. They differ in their depositional environment, basin depozones and reflect successive stages of the basin's evolution. Depositional unit I is represented by lagoon-estuary and barred coastline deposits (backbulge and forebulge depozones) and reflects the Pre- to Early transgressive phase over the pre-Cenozoic bedrock. The deposition was influenced by reactivation of the basement faults due to the Early Styrian phase of thrusting (Ottnangian–Early Karpatian). The source from the "local" crystalline basement formed by crystalline rocks of the

Brunovistulicum played an important role here. The second depositional unit is represented by the coastline to shallow marine deposits (forebulge depozone), reflecting the Karpatian transgression (TB 2.2. sea-level cycle), which drowned the embayed passive margins of the basin. Continued cratonward shift of the facies belts is typical for this unit. Tidalites (tidal flat deposits) recognized within this unit represent the only described tide-generated deposits of the Carpathian Foredeep basin in Moravia. The source from the basin passive margin (especially from greywackes and conglomerates of the Moravian–Silesian Paleozoic deposits/Culm unit) has been proved. The third depositional unit is formed by offshore deposits and represents a foredeep depozone. The provenance from both passive and active basin margin (Silesian Unit of the Western Carpathian Flysch Zone) has been proved. The cratonward forebulge flexural retreat continued. The succession of depositional units reflects both a stepwise migration of the foredeep basin axis and shift of basin depozones outwards/cratonwards, together with the forebulge retreat. The shift of the foreland basin depozones more than 50 km cratonward can be assumed. The basin was significantly enlarged and its bathymetry changed.

Renewed thrusting (Late Styrian phase of thrusting–Late Karpatian) led, in the most proximal/inner part of the basin, to tectonic deformation of the basin infill and its partial incorporation into the thrusts. Generally westward advance of the nappes led to shift of the lithosphere flexure cratonward and the basin subsidence axis northwestward of the area under study. The inner part of the basin was buried under the nappes or destroyed. The deposition in the foreland basin continued only in the flexed periphery in front of the nappes, so the basin was narrower and deeper.

The complete reconstruction of the basin's shape, position, and lateral extent are all interpreted as a consequence of the phases of the thrust-sheet stacking and sediment loading in combination with eustatic sea-level change.

Acknowledgements: The study is the result of specific research at Institute of Geological Sciences of Masaryk University. The authors thank Moravian Oil Mines Inc. which provided the primary data. Proof-Reading-Service kindly improved the written English of the manuscript. We also give thanks to three anonymous reviewers and editor Michal Kováč for their helpful comments and suggestions.

References

Adámek J., Brzobohatý R., Pálenský P. & Šikula J. 2003: The Karpatian in the Carpathian Foredeep (Moravia). In: Brzobohatý R., Cicha I., Kováč M. & Rögl F. (Eds.): The Karpatian, a Lower Miocene Stage of the Central Paratethys. *Masaryk University,* Brno 75–92.

Adegoke A.K., Abdullah W.H., Hakimi M.H. & Yandoka B.M.S. 2014: Geochemical characterisation of Fika Formation in the Chad (Bornu) Basin, northeastern Nigeria: Implications for depositional environment and tectonic setting. *Appl. Geochem.* 43, 1–12.

Ali S., Stattegger K., Garbe-Schönberg D., Frank M., Kraft S. & Kuhnt W. 2014: The provenance of Cretaceous to Quaternary sediments in the Tarfaya basin, SW Moroco: Evidence from trace element geochemistry and radiogenic Nd-Sr isotopes. *J. Afr. Earth Sci.* 90, 64–76.

Andersson P.O.D., Worden R.H., Hodgson D.M. & Flint S. 2004: Provenance evolution and chemostratigraphy of a Palaeozoic submarine fan-complex: Tanqua Karoo Basin, South Africa. *Mar. Petrol. Geol.* 21, 555–577.

Bahlburg H. 1998: The geochemistry and provenance of Ordovician turbidites in the Argentinian Puna. In: Pankhurst R.J. & Rapela C.W. (Eds.): The Proto-Andean Margin of Gondwana. *Geol. Soc. London, Spec. Publ.* 142, 127–142.

Beaumont C., Quinlan G.M. & Stockmal G.S. 1993: The evolution of the Western Interior Basin: causes, consequences and unsolved problems. In: Caldwell W.G.E. & Kauffman E.G. (Eds.): Evolution of the Western Interior Basin. *Geol. Assoc. Can. Spec. Paper* 39, 97–117.

Benada S. 1986: New findings on the extension of the paraauthochtonous deposits of Karpatian in the central part of the Carpathian Neogene Foredeep in Moravia. *Zemní Plyn Nafta* 31, 4, 485–492 (in Czech).

Benada S. & Kokolusová A. 1987: The new knowledge about the geological positions of the coarse-grained clastic deposits of the Karpatian in the Central part of the Carpathian Foredeep. *Zemní Plyn Nafta* 32, 1, 1–15 (in Czech).

Bergman K.M. & Walker R.G. 1988: Formation of Cardium Erosion surfaces E5, and associated deposition of conglomerate: Carrot Creek field, Cretaceous Western Interior Seaway, Alberta. In: James D.P.& Leckie D.A. (Eds.): Sequences, Sedimentology, Surface and Subsurface. *Canad. Soc. Petrol. Geol., Memoir* 15, 15–24.

Bhatia M.R. & Crook A.W. 1986: Trace element characteristics of graywackes and tectonic setting discrimination of sedimentary basins. *Contr. Mineral. Petrology* 92, 181–193.

Bieg U., Nebelsick J.H. & Rasser M. 2007: North Alpine Foreland Basin (Upper Marine Molasse) of Southwest Germany: Sedimentology, Stratigraphy and Palaeontology. *Geol. Alp* 4, 149–158.

Bieg U., Süss M.P. & Kuhlemann J. 2008: Simulation of tidal flow and circulation patterns in the Early Miocene (Upper Marine Molasse) of the Alpine foreland basin. *Spec. Publ. Int. Ass. Sediment.* 40, 145–169.

Borges J. & Huh Y. 2007: Petrography and chemistry of the bed sediments of the Red River in China and Vietnam: Provenance and chemical weathering. *Sed. Geol.* 194, 155–168.

Brzobohatý R. & Cicha I. 1993: The Carpathian Foredeep. In: Přichystal A. et al. (Eds.): The Geology of the Moravia and Silesia. *MZM a PřF MU,* Brno, 123–128 (in Czech).

Bubík M. & Dvořák J. 1996: About the finding of the Karpatian (Miocene) and other results of the Slatinky MH-10 borehole. *Zpr. geol. výzk. v r. 1995* 20–21 (in Czech).

Cattaneo A. & Steel R.J. 2003. Transgressive deposits: a review of their variability. *Earth-Sci. Rev.* 62, 187–228.

Catuneanu O., WilliS A.J. & Miall A.D. 1998: Temporal significance of sequence boundaries. *Sed. Geol.* 121, 157–178.

Clifton H.E. 1976: Wave-formed sedimentary structures - a conceptual model. In: Davis R.A. & Ethington R.L. (Eds.): Beach and Nearshore processes. *SEPM Spec. Publ.* 24, 126–148.

Cogan J., Lerche I., Dorman J.T. & Kanes W. 1993: Flexural plate inversion: application to the Carpathian Foredeep, Czechoslovakia. *Mod. Geol.* 17, 355-392.

Corcoran P.L. 2005: Recycling and chemical weathering in tectonically controlled Mesozoic-Cenozoic basins of New Zealand. *Sedimentology* 52, 757–774.

Cox R. & Lowe D.R. 1995: A conceptual review of regional-scale

controls on the composition of clastic sediment and the co-evolution of continental blocks and their sediment cover. *J. Sed. Res.* A65, 1, 1–12.

Crampton S.L. & Allen P.A. 1995: Recognition of forebulge unconformities associated with early stag foreland basin development: example from the North Alpine foreland basin. *AAPG Bulletin* 79, 1495–1514.

Čopjaková R. 2007: The reflection of provenance changes in the psefitic and psamitic sedimentary fraction of the Myslejovice Formation (heavy mineral analysis). *PhD thesis, Masaryk University,* Brno, 1–137 (in Czech).

Čopjaková R., Sulovský P. & Otava J. 2002: Comparison of the chemistry of detritic pyrope-almandine garnets of the Luleč Conglomerates with the chemistry of granulite garnets from the Czech Massif. *Geol. výzk. Mor. Slez. v r. 2001* 44–47 (in Czech).

Čopjaková R., Sulovský P. & Paterson B.A. 2005: Major and trace elements in pyrope–almandine garnets as sediment provenance indicators of the Lower Carboniferous Culm sediments, Drahany Uplands, Bohemian Massif. *Lithos* 82, 51–70.

Dalrymple R.W. & Choi K. 2007: Morphologic and facies trends through the fluvial–marine transition in tide-dominated depositional systems: A schematic Framework for environmental and sequence-stratigraphic interpretation. *Earth Sci. Rev.* 81, 135–174.

Dalrymple R.W., Zaitlin B.A. & Boyd R. 1992: Estuarine facies models: conceptual basis and stratigraphic implications. *J. Sed. Petrology* 62, 1130–1146.

DeCelles P.G. & Giles K.A. 1996: Foreland basin systems. *Basin Res.* 8, 105–123.

Dickinson W.R. 1985: Interpreting provenance relations from detrital modes of sandstones. In: Zuffa G.G. (Ed.): Provenance of Arenites. *D. Reidel Publication Co.*, 333–361.

Dickinson W.R., Beard L.S., Brakenridge G.R., Erjavec J.L., Ferguson R.C., Inman K.F., Knepp R.A., Lindberg F.A. & Ryberg P.T. 1983: Provenance of North American Phanerozoic sandstones in relation to tectonic setting. *Geol. Soc. Amer. Bull.* 94, 222-235.

Dickinson W.R. & Suczek C.A 1979: Plate tectonics and sandstone composition. *Amer. Assoc. Petrol. Geol. Bull.* 63, 2164–2182.

Dott R.H. & Bourgeois J. 1982: Hummocky stratification: Significance of its variable bedding sequences. *Geol. Soc. Amer. Bull.* 93, 663–680.

Drake D.E. & Cacchione D.A. 1985: Seasonal variation in sediment transport on the Russian River shelf, California. *Cont. Shelf Res.* 4, 495–514.

Duke W.L. 1985: Hummocky cross-stratification, tropical hurricanes, and intense winter storms (palaeogeography). *Sedimentology* 32,167–194.

Duke W.L., Arnott R.W.C. & Cheel R.J. 1991: Shelf sandstones and hummocky cross-stratification: new insights on a stormy debate. *Geology* 19, 625–628.

Eliáš M. & Pálenský P. 1998: The model for the development of the Miocene foredeeps in the Ostrava area. *Zpr. geol. výzk. v r. 1997*, 65–66 (in Czech).

Fedo C.M., Nesbitt H.W. & Young G.M. 1995: Unraveling the effects of potassium metasomatism in sedimentary rocks and paleosols, with implications for paleoweathering conditions and provenance. *Geology* 23, 921–924.

FitzGerald D., Buynevich I. & Hein C. 2012: Morphodynamics and facies architecture of tidal inlets and tidal deltas. In: Davis J.A. Jr. & Dalrymple R.W. (Eds.): Priciples of Tidal Sedimentology. *Springer*, New York, 301–333.

Flemings P.B. & Jordan T.E. 1989: A synthetic stratigraphic model of foreland basin development. *J. Geophys. Res.* 94, B4, 3851–3866.

Flemings P.B. & Jordan T.E. 1990: Stratigraphic modelling of foreland basins: Interpreting thrust deformation and lithosphere rheology. *Geology* 18, 430–434.

Fralick P.W. & Kronberg B.I. 1997: Geochemical discrimination of clastic sedimentary rock sources. *Sed. Geol.* 113, 111–124.

Galloway W.E. & Hobday D.K. 1996: Terrigenous Clastic Depositional Systems: Applications to Fossil Fuel and Groundwater Resources, 2nd edition. New York, *Springer*, 1–489.

Gilíková H., Otava J. & Stráník Z. 2002: Petrological characteristics of sediments of the Magura Flysch at the map-sheet Holešov. *Geol. výzk. Mor. Slez. v r. 2001*, 26–29 (in Czech).

Gu X.X, Liu J.M., Zheng M.H., Tang J.X. & Qi L. 2002: Provenance and tectonic setting of the Proterozoic turbidites in Hunan, South China: geochemical evidence. *J. Sed. Res.* 72, 393–407.

Gupta S. 1999: Controls on sedimentation in distal margin pallaeovalleys in the Early Tertiary Alpine foreland basin, southeastern France. *Sedimentology* 46, 357–384.

Haq B.U., Hardenbol J. & Vail P.R. 1988: Mesozoic and Cenozoic chronostratigraphy and cycles of sea-level change. In: Wilgius C.K. et al. (Eds.): Sea-Level Changes. *SEMP Spec. Publ.* 42, 71–108.

Helland-Hansen W. & Gjelberg J.G. 1994: Conceptual basis and variability in sequence stratigraphy: a different perspective. *Sed. Geol.* 92, 31–52.

Heller P.L., Angevinw C.L., Winslow N.S. & Paola C. 1988: Two-phases stratigraphic model of forelad-basin sequences. *Geology* 16, 501–504.

Hiscott R.N. 1984: Ophiolitic Source Rocks for Taconic-Age Flysch: Trace-Element Evidence. *Geol. Soc. Amer. Bull.* 95, 1261–1267.

Hladilová S., Nehyba S., Dolákova N. & Hladíková J. 1999: Comparison of some relics of Miocene sediments on the eastern margin of the Bohemian Massif. *Geol. Carpathica* 50, Spec. Iss., 31–33.

Hladilová Š., Nehyba S., Zágoršek K., Tomanová Petrová P., Bitner M.A. & Demeny A. 2014: Early Badenian transgression on the outer flank of Western Carpathian Foredeep, Hluchov area, Czech Republic. *Ann. Soc. Geol. Pol.* 84, 259–279.

Hohenegger J., Ćorić S. & Wagreich M. 2014: Timing of the Middle Miocene Badenian Stage of the Central Paratethys. *Geol. Carpathica* 65, 1, 55–66.

Hohenegger J., Rögl F., Ćorić S., Pervesler P., Lirer F., Roetzel R., Scholger R. & Stingl K. 2009: The Styrian Basin: A key to the Middle Miocene (Badenian/Langhian) Central Paratethys transgressions. *Austrian J. Earth Sci.* 102, 103–132.

Holcová K., Brzobohatý R., Kopecká J. & Nehyba S. 2015: Reconstruction of the unusual Middle Miocene (Badenian) palaeoenvironment of the Carpathian Foredeep (Lomnice/Tišnov denudational relict, Czech Republic) *Geol. Quarterly* 59, 654–678.

Hubert J.F. 1962: A zircon–tourmaline–rutile maturity index and the interdependance of the composition of heavy mineral assemblages with the gross composition and texture of sandstones. *J. Sed. Petrol.* 32, 440–450.

Ingersoll R.V. 1990: Actualistic sandstones petrofacies: discriminating modern and ancient source rocks. *Geology* 18, 733–736.

Johnson D.D. & Beaumont C. 1995: Preliminary results from a planform kinematic model of orogen evolution, surface processes and the development of clastic foreland basin stratigraphy. In: Dorobek S.L. & Ross G.M. (Eds.): Stratigraphic Evolution of Foreland Basins. *Spec. Publ. Soc. Econ. Paleont. Mineral.* 52, 3–24.

Jordan T.E. & Flemings P.B. 1991: Large-scale stratigraphic architecture, eustatic variation, and unsteady tectonism: a theoretical evaluation. *J. Geophys. Res.* 96, B4, 6681–6699.

Kalvoda J., Bábek O., Fatka O., Leichmann J., Melichar R., Nehyba S. & Špaček P. 2008: Brunovistulian terrane (Bohemian Massif, Central Europe) from late Proterozoic to late Paleozoic: a review. *Int. J. Earth Sci.* 97, 3, 497–517.

Kalvoda J., Leichmann J., Bábek O. & Melichar R. 2003: Brunovistulian terrane (Central Europe) and Istanbul zone (NW Turkey): Late proterozoic and paleozoic tectonostratigraphic development and paleogeography. *Geol. Carpathica* 54, 3, 139–152.

Kempf O. & Pfiffner A. 2004: Early Tertiary evolution of the North Alpine Foreland Basin of the Swiss Alps and adjoining areas. *Basin Res.* 16, 549–567.

Koss J.E., Ethridge F.G. & Schumm S.A. 1994: An experimental study of the effect of base-level change on fluvial, coastal and shelf systems. *J. Sed. Res*. B64, 90–98.

Kováč M. 2000: Geodynamic, paleogeographical and structural development of the Miocene Carpatho-Pannonian region. New view on the Slovak Neogene basins. *Veda,* Bratislava, 1–176 (in Slovak).

Kováč M., Sergeyevna A.-G., Brzobohatý R., Fodor L., Harzhauser M., Oszczypko N., Pavelić D., Rögl F., Saftić B., Sliva Ľ. & Stráník Z. 2003: Karpatian paleogeography, tectonics and eustatic changes. In: Brzobohatý R. et al. (Eds.): The Karpatian, A Lower Miocene Stage of the Central Paratethys. *Masaryk University,* Brno, 49–72.

Kováč M., Grygorovich A.A., Bajraktarević Z., Brzobohatý R., Filipescu S., Fodor L., Harzhauser M., Oszczypko N., Pavelić D., Rögl F., Saftić B., Sliva Ľ., Kvaček Z., Hudáčková N. & Slamková M. 2004: Paleogeography of Central Paratethys during the Karpatian and Badenian. *Scripta Fac. Sci. Nat. Univ. Masaryk Brunensis*, *Geology* 31–32, 7–17.

Krzywiec P. 2001: Contrasting tectonic and sedimentary history of the central and eastern parts of the Polish Carpathian foredeep basin — results of seismic data interpretation. *Mar. Petrol. Geol.* 18, 13–38.

Kukal Z. 1986: Manual of practical sediment nomenclature and classification. *Czech Geol. Surv.*, Praha, 1–80 (in Czech).

Leszczyński S. & Nemec W. 2014: Dynamic stratigraphy of composite peripheral unconformity in a foredeep basin. *Sedimentology* 62, 3, 645–680.

Li C. & Yang S. 2010: Is chemical index of alteration (CIA) a reliable proxy for chemical weathering in global drainage basins? *Amer. J. Sci.* 310, 111–127.

Lis P. & Wysocka A. 2012: Middle Miocene deposits in Carpathian Foredeep: facies analysis and implications for hydrocarbon reservoir prospecting. *Ann. Soc. Geol. Pol.* 82, 239–253.

McLennan S.M. 1993: Weathering and global denudation. *J. Geology* 101, 295–303.

McLennan S.M., Heming S.R., McDaniel D.K. & Hanson G.N. 1993: Geochemical approaches to sedimentation, provenance, and tectonics. In: Johnsson M.J. & Basu A. (Eds.): Processes controlling the composition of clastic sediments. *Geol. Soc. Amer., Spec. Pap.* 284, 1–19.

Meinhold G., Anders B., Kostopoulos D. & Reischmann T. 2008: Rutile chemistry and thermometry as provenance indicator: An example from Chios Island, Greece. *Sed. Geol.* 203, 98–111.

Meinhold G. 2010: Rutile and its applications in earth sciences. *Earth Sci Rev.* 102, 1–28.

Miall A.D. 1989: Architectural elements and bounding surfaces in channelized clastics deposits: notes on comparisons between fluvial and turbidite systems. In: Taira A. & Masuda F. (Eds.): Sedimentary Facies in the Active Plate Margin. *Terra Sci. Publ. Company* 3–15.

Milliken K.L. 1988: Loss of provenance information through subsurface diagenesis in Plio-Pleistocene sediments, northern Gulf of Mexico. *J. Sed. Petrology* 58, 992–1002.

Morton A.C. 1984: Stability of detrital heavy minerals in Tertiary sandstones from the North Sea Basin. *Clay Miner.* 19, 287–308.

Morton A.C. 1991: Geochemical studies of detrital heavy minerals and their application to provenance studies. In: Morton A.C. et al. (Eds.): Developments in Sedimentary Provenance Studies. *Geol. Soc. London, Spec. Publ.* 57, 31–45.

Morton A.C. & Hallsworth C.R. 1994: Identifying provenance-specific features of detrital heavy mineral assemblages in sandstones. *Sed. Geol.* 90, 241–256.

Morton A.C. & Hallsworth C.R. 1999: Processes controlling the composition of heavy mineral assemblages in sandstones. *Sed. Geol.* 124, 3–29.

Morton A.C., Hallsworth C.R. & Chalton B. 2004: Garnet compositions in Scottish and Norwegian basement terrains: a framework for interpretation of North Sea sandstone provenance. *Mar. Petrol. Geol.* 21, 393–410.

Nehyba S. 2000: The cyclicity of Lower Miocene deposits of the SW part of the Carpathian Foredeep as the depositional response to sediment supply and sea-level changes. *Geol. Carpathica* 51, 1, 7–17.

Nehyba S. & Buriánek D. 2004: Chemistry of garnet and tourmaline — contribution to provenance studies of fine grained Neogene deposits of the Carpathian Foredeep. *Acta Mus. Moraviae, Sci. Geol.* 89, 149–159 (in Czech).

Nehyba S. & Petrová P. 2000: Karpatian sandy deposits in the southern part of the Carpathian Foredeep in Moravia. *Věstník Čes. Geol. Úst.* 75, 1, 53–66.

Nehyba S. & Roetzel R. 2010: Fluvial deposits of the St. Marein-Freischling Formation — insights into initial depositional processes on the distal external margin of the Alpine-Carpathian Foredeep in Lower Austria. *Austrian J. Earth Sci.* 103, 2, 50–80.

Nehyba S. & Šikula J. 2007: Depositional architecture, sequence stratigraphy and geodynamic development of the Carpathian Foredeep (Czech Republic). *Geol. Carpathica* 58, 1, 53–69.

Nehyba S., Roetzel R. & Maštera L. 2012: Provenance analysis of the Permo–Carboniferous fluvial sandstones of the southern part of the Boskovice Basin and the Zöbing Area (Czech Republic, Austria): implications for paleogeographical reconstructions of the post-Variscan collapse basins. *Geol. Carpathica* 63, 5, 365–382.

Nemec W. 2005: Principles of lithostratigraphic logging and facies analyses. *Institut for geovitenskap, Univ. Bergen*, 1–28.

Nesbitt H.W. 1979: Mobility and fractionation of rare earth elements during weathering of granodiorite. *Nature* 279, 206–210.

Nesbitt H.W. & Young G.M. 1982: Early Proterozoic climates and plate motions inferred from major element chemistry of lutites. *Nature* 299, 715–717.

Nesbitt H.W. & Young G.M. 1989: Formation and diagenesis of weathering profiles. *J. Geology* 97, 129–147.

Nesbitt H.W. & Young G.M. 1998: Processes controlling the distribution of Ti and Al in weathering profiles, siliciclastic sediments and sedimentary rocks. *J. Sed. Res.* 68, 3, 448–455.

Nesbitt H.W., Young G.M., McLennan S.M. & Keays R.R. 1996: Effects of chemical weathering and sorting on the petrogenesis of siliciclastic sediments, with implications for provenance studies. *J. Geology* 104, 525–542.

Nittrouer C.A., DeMaster D.J., Kuehl S.A. & McKee B.A. 1986: Association of sand with mud deposits accumulating on continental shelves. In: Knight R.J. & McLean J.R. (Eds.): Shelf Sands and Sandstones. *Canad. Soc. Petrol. Geol., Memoir* 11*,* 17–25.

Oszczypko N., Krzywiec P., Popadyuk I. & Peryt T. 2006: Carpathian Foredeep Basin (Polish and Ukraine): Its sedimentary,

structural, and geodynamic evolution. In: Golonka J. & Picha F.J. (Eds.): The Carpathians and Their Foreland: Geology and Hydrocarbon Resources. *AAPG Memoir* 84, 293–350.

Oszczypko N. & Oszczypko-Clowes M. 2012: Stages of development in the Polish Carpathian Foredeep Basin. *Central Eur. J. Geosci*. 4, 1, 138–162.

Otava J. 1998: Trends of changes in the composition of siliciclastics of the Lower Carboniferous at Drahany Upland (Moravia) and their geotectonic interpretation. *Geol. výzk. Mor. Slez. v r. 1997*, 62–64 (in Czech).

Otava J., Krejčí O. & Sulovský P. 1997: First results of electron microprobe analyses of detrital garnets from the Rača Unit of the Magura Group. *Geol. výzk. Mor. Slez. v r. 1996*, 39–42 (in Czech).

Otava J., Sulovský P. & Kejčí O. 1998: The results of study of the detrital garnets from the Cretaceous sediments of the Rača Unit of the Magura Group (Outer Carpathians). *Geol. výzk. Mor. Slez. v r. 1997*, 29–31 (in Czech).

Otava J., Sulovský P. & Čopjaková O. 2000: Provenance changes of the Drahany Culm greywackes: statistical evaluation. *Geol. výzk. Mor. Slez. v r. 1999*, 94–98 (in Czech).

Passchier S. & Whitehead J.M. 2006: Anomalous geochemical provenance and weathering history of Plio–Pleistocene glaciomarine fjord strata, Bardin Bluffs Formation, East Antarctica. *Sedimentology* 53, 929–942.

Petránek J. 1963: Sedimentary rocks. *Czech Academy of Sciences*, Praha, 1–717 (in Czech).

Plint A.G. 2000: Sequence stratigraphy and paleogeography of a Cenomanian deltaic complex: The dunvegan and lower kaskapau formations in subsurface and outcrop, Alberta and British Columbia, Canada. *Bull. Canad. Petrol. Geol.* 48, 43–79.

Plint A.G., Hart B. & Donaldson W.S. 1993: Lithospheric flexure as a control on stratal geometry and facies distribution in Upper Cretaceous rocks of the Alberta Foreland Basin. *Basin Res.* 5, 69–77.

Plint A.G., McCarthy P.J. & Faccini U.F. 2001: Nonmarine sequence stratigraphy: Updid expression of sequence boundaries and systems tracts in a high-resolution framework, Cenomanian Dunvegan Formation, Alberta foreland basin, Canada. *AAPG Bulletin* 85, 1967–2001.

Posamentier H.W., Allen G.P., James D.P. & Tesson M. 1992: Forced regressions in a sequence stratigraphic framework: concept, examples, and exploration significance. *AAPG Bulletin* 76, 1687–1709.

Reading H.G. 1996: Sedimentary environments: processes, facies and stratigraphy. *Blackwell Science*, Oxford, 1–704.

Reineck H.E. & Singh I.B. 1973: Depositional sedimentary environments: with reference to terrigenous clastics. *Springer-Verlag*, Berlin, 1–439.

Reynand J.-Y. & Dalrymple R.W. 2012: Shallow-marine tidal deposits. In: Davis J.A. Jr. & Dalrymple R.W. (Eds.): Priciples of Tidal Sedimentology. *Springer*, New York, 335–369.

Rider M.H. 1986: The geological interpretation of well logs. *John Wiley & Sons*, New York, 1–175.

Roser B.P. & Korsch R.J 1999: Geochemical characterization, evolution and source of Mesozoic accretionary wedge: the Torlesse terrane, New Zealand. *Geol. Mag.* 136, 493–512.

Roser B.P., Cooper R.A., Nathan S. & Tulloch A.J. 1996: Reconnaissance sandstone geochemistry, provenance, and tectonic setting of the lower Paleozoic terranes of the West Coast and Nelson, New Zealand. *New Zeal. J. Geol. Geop.* 39, 1–16.

Ross D.J.K. & Bustin R.M. 2009: Investigating the use of sedimentary geochemical proxies for paleoenvironment interpretation of thermally mature organic-rich strata: Examples from the Devonian–Mississippian shales, Western Canadian Sedimentary Basin. *Chem. Geol.* 260, 1–19.

Sacchi M., Molisso F., Pacifico A., Vigliotti M., Sabbarese C. & Ruberti D. 2014: Late-Holocene to recent evolution of Lake Patria, South Italy: An example of a coastal laggon within a Mediterranean delta system. *Global Planet Change* 117, 9–27.

Salata D. 2004: Garnet provenance in mixed first-cycle and polycycle heavy-mineral assamblages of the Ropianka and Menilite Formations (Skole Nappe, Polish Flysch Carpathians): constraints from chemical composition and grain morphology. *Ann. Soc. Geol. Pol.* 83, 161–177.

Salata D. 2013a: Detrital garnets from the Upper Cretaceous–Palaeocene sandstones of the Polish part of the Magura nappe and the Pieniny Klippen Belt: chemical constraints. *Ann. Soc. Geol. Pol.* 74, 351–364.

Salata D. 2013b: Source rocks for heavy minerals in lower part of Menilite Formation of Skole Nappe (Polish Flysch Carpathians), based on study of detrital garnet and tourmaline. *Ann. Soc. Geol. Pol.* 83, 1–17.

Sen S., Das P.K., Bhagaboty B & Singha L.J.C. 2012: Geochemistry of shales of Barail group occurring in and around Mandardisa, North Catchar Hills, Assam; India: Its implications. *Int. J. Chem. Appl. (IJCA)* 4, 1, 25–37.

Shanley K.W. & McCabe P.J. 1994: Perspectives on the sequence stratigraphy of continental strata. *AAPG Bulletin* 78, 544–568.

Sinclair H.D., Coakley B.J., Allen P.A. & Watts A.B. 1991: Simulation of foreland basin stratigraphy using a diffusion model of mountain belt uplift and erosion: an example from the central Alps, Switzerland. *Tectonics* 10, 3, 599–620.

Stráník Z., Hrouda F., Otava J., Gilíková H. & Švábenická L. 2007: The Upper Oligocene–Lower Miocene Krosno lithofacies in the Carpathian Flysch Belt (Czech Republic): sedimentology, provenance and magnetic fabrics. *Geol. Carpathica* 58, 4, 321–332.

Suggate S.M. & Hall R. 2013: Using detrital garnet compositions to determine provenance: a new compositional database and procedure. In: Scott. R.A. et al. (Eds.): Sediment Provenance Studies in Hydrocarbon Exploration and Production. *Geol. Soc. London, Spec. Publ.* 386, 373–393.

Suttner L.J. & Dutta P.K. 1986: Alluvial sandstone composition and paleoclimate, I. framework mineralogy. *J. Sed. Petrology* 56, 3, 329–345.

Swift D.J.P., Philips S. & Thorne J.A. (1991): Sedimentation on continental margins: V. Parasequences. In: Swift D.J.P. et al. (Eds.): Shelf Sand and Sandstone Bodies: Geometry, Facies and Sequence Stratigraphy. *Spec. Publ. Int. Assoc. Sediment.* 14, 153–187.

Sztanó O. & de Boer P.L. 1995: Basin dimensions and morphology as controls an amplification of tidal motions (the Early Miocene North Hungarian Bay). *Sedimentology* 42, 665–682.

Šikula J. & Nehyba S. 2006: Interpretation of the Neogene deposits from the area Vizovice Hills according the subsurface data. *Geol. výzk. Mor. Slez. v r. 2005*, 54–57 (in Czech).

Taylor S.R. & McLennan S.M. 1985: The Continental Crust: Its Composition and Evolution. *Blackwell*, London, 1–312.

Thonová H., Holzknecht M., Krystek I. & Brzobohatý R. 1987: New insights into the development of Karpatian under flysch nappes in the section „Center". *Zemní Plyn Nafta* 32, 3, 383–389 (in Czech).

Tomkins H.S., Powell R. & Ellis D.J. 2007: The pressure dependence of the zirkonium-in-rutile thermometer. *J. Metamorph. Geology* 25, 703–713.

von Eynatten H., Barceló-Vidal C. & Pawlowsky-Glahn V. 2003: Modelling compositional changes: the example of chemical weathering of granitoid rocks. *Math. Geology* 35, 3, 231–251.

Walker R.G. & James N.P. 1992: Facies models: Response to sea level change. *Geol. Assoc. Canada*, 1–380.

Walker R.G. & Plint A.G. 1992: Wave- and storm-dominated shallow marine systems. In: Walker R.G. & James N.P. (Eds.): Facies Models: Response to Sea Level Change. *Geol. Assoc. Canada*, 219–238.

Waśkowska A., Cieszkowski M., Golonka J. & Kowal-Kasprzyk J. 2014: Paleocene sedimentary record of ridge geodynamics in Outer Carpathian basin (Subsilesian Unit). *Geol. Carpathica* 65, 1, 35–54.

Watson E.B., Wark D.A. & Thomas J.B. 2006: Crystallization thermometers for zircon and rutile. *Contrib. Mineral. Petrol.* 151, 413–433.

Wright L.D., Chappel J., Bradshaw M.P. & Cowell P. 1979: Morphodynamics of reflective and dissipative beach and nearshore systems, southeastern Australia. *Mar. Geol.* 32, 105–140.

Yang Y. & Miall A.D. 2010: Migration and stratigraphic fill of an underfilled foreland basin: Middle–Late Cenomanian Belle Fourche Formation in southern Alberta, Canada. *Sed. Geol.* 227, 1–4, 51–64.

Zack T., Moraes R. & Kronz A. 2004a: Temperature dependence of Zr in rutile: empirical calibration of rutile thermometer. *Contrib. Mineral. Petrol.* 148, 471–488.

Zack T., von Eynatten H. & Kronz A. 2004b: Rutile geochemistry and its potential use in quantitative provenance studies. *Sed. Geol.* 171, 37–58.

Zádrapa M. 1979: Heavy minerals in the Karpatian deposits in the Central and Southwestern parts of the Carpathian Foredeep in the Moravia. *Zemní Plyn Nafta* 24, 3, 447–451 (in Czech).

Zágoršek K., Nehyba S., Tomanová Petrová P., Hladilová Š., Bitner M.A., Doláková N., Hrabovský J. & Jašková V. 2012. Local catastrophe near Přemyslovice (Moravia, Czech Republic) during Middle Miocene due to the tephra input. *Geol. Quarterly* 56, 269–284.

Zaitlin B.A., Dalrymple R.W. & Boyd R. 1994: The stratigraphic organization of incised-valley systems associated with relative sea-level change. In: Dalrymple R.W. et al. (Eds.): Icised-Valley Systems: Origin and Sedimentary Sequences. *SEPM Spec. Publ.* 51, 45–60.

Zhang K.-J. 2004: Secular geochemical varitions of the Lower Cretaceous siliciclastic rocks from central Tibet (China) indicate a tectonic transition from continental collision to back-arc rifting. *Earth Planet. Sci. Lett.* 229, 73–89.

Zimmermann U. & Bahlburg H. 2003: Provenance analysis and tectonic setting of the Ordovician clastic deposits in the southern Puna Basin, NW Argentina. *Sedimentology* 50, 1079–1104.

Zuffa G.G. 1980: Hydrid arenites: Their composition and classification. *J. Sed. Petrology* 50, 21–29.

Zuffa G.G. 1985: Optical analyse of arenites: influence of methodology on compositional results. In: Zuffa G.G. (Ed.): Provenance of Arenites. *D. Reidel Publication Co.*, 165–189.

Zuschin M., Harzhauser M., Hengst B., Mandic O. & Roetzel R. 2014: Long-term ecosystem stability in an Early Miocene estuary. *Geology* 42, 1–4.

Electronic supplement

Appendix 1: The major element composition (wt. %) of the studied samples.

Sample (borehole)	SiO_2	Al_2O_3	Fe_2O_3	MgO	CaO	Na_2O	K_2O	TiO_2	P_2O_5	MnO	Cr_2O_3	LOI
BAR1	53.05	11.73	4.56	3.45	8.12	1.17	2.61	0.57	0.13	0.08	0.014	14.3
BAR1	51.77	12.25	4.81	3.60	8.27	1.03	2.52	0.56	0.11	0.13	0.013	14.7
BAR1	54.16	15.70	5.11	2.06	4.08	0.91	2.80	0.74	0.13	0.03	0.017	14.1
BAR1	53.27	11.97	4.62	3.50	8.15	1.14	2.43	0.57	0.14	0.08	0.014	13.9
G1	70.88	5.13	2.15	2.53	6.96	0.90	1.11	0.27	0.09	0.05	0.004	9.9
G1	52.61	16.22	5.68	3.55	5.03	1.31	3.44	0.80	0.15	0.06	0.020	10.9
G1	68.16	6.57	2.71	2.29	8.23	1.25	1.16	0.50	0.09	0.08	0.007	8.9
G1	65.85	5.62	2.78	2.82	8.87	1.25	0.86	0.50	0.09	0.09	0.007	11.2
G1	54.44	14.90	4.98	3.29	5.88	1.19	3.17	0.73	0.14	0.06	0.016	11.0
G1	74.03	5.51	2.01	2.20	6.00	1.18	1.04	0.38	0.09	0.06	0.006	7.4
G2	49.97	14.47	5.17	3.10	7.82	0.89	2.99	0.57	0.16	0.04	0.017	14.6
G2	45.08	14.37	4.84	2.50	10.81	0.89	2.93	0.60	0.21	0.04	0.016	17.5
G2	50.88	17.57	5.54	3.74	4.91	1.28	3.84	0.80	0.14	0.06	0.019	11.0
G2	52.71	16.05	5.55	3.36	4.64	0.98	3.36	0.61	0.18	0.04	0.018	12.2
G2	48.87	16.15	6.06	3.58	6.62	0.92	3.49	0.70	0.12	0.06	0.018	13.2
G2	44.27	13.97	4.65	2.44	11.88	0.75	2.79	0.59	0.18	0.04	0.015	18.2
G2	49.39	19.39	5.67	4.09	3.21	1.06	4.85	0.85	0.18	0.04	0.022	11.0
G2	48.90	15.46	5.70	3.20	6.35	0.90	3.27	0.64	0.24	0.04	0.018	15.0
G3	49.44	16.56	5.99	3.68	5.55	1.07	3.82	0.77	0.12	0.06	0.020	12.7
G3	52.73	14.99	5.62	3.43	6.19	1.32	3.30	0.74	0.15	0.06	0.017	11.3
HOL1	48.06	15.05	5.19	2.41	8.22	0.88	2.82	0.64	0.15	0.04	0.018	16.3
HOL1	50.26	14.02	5.32	3.75	6.96	1.02	2.84	0.62	0.12	0.08	0.016	14.8
HOL1	60.02	9.41	3.53	3.15	8.39	1.21	1.98	0.52	0.12	0.08	0.010	11.4
HOL1	56.60	11.69	4.52	2.85	7.30	1.07	2.45	0.57	0.11	0.07	0.011	12.6
HOL1	56.61	12.10	4.36	2.62	7.20	1.00	2.51	0.57	0.09	0.06	0.012	12.7
HOL1	58.04	11.72	4.22	2.67	6.88	1.06	2.49	0.57	0.11	0.06	0.009	12.0
HOL1	57.22	14.33	5.32	2.95	3.59	1.08	2.76	065	0.10	0.06	0.013	11.8
HOL1	59.98	7.16	3.09	2.72	11.05	1.14	1.59	0.41	0.12	0.14	0.007	12.3
HOL1	63.32	9.32	3.34	2.20	6.89	1.07	2.26	0.46	0.12	0.06	0.006	10.8
HOL1	56.30	15.12	5.67	3.00	2.50	1.09	2.89	0.68	0.11	0.05	0.013	12.4
HOL1	59.84	9.25	3.72	3.08	8.40	1.20	1.93	0.53	0.16	0.11	0.009	11.4
HUL2	57.31	12.13	4.50	3.08	6.66	1.17	2.56	0.59	0.13	0.07	0.014	11.6
HUL2	45.34	14.09	4.92	2.88	10.04	0.84	2.88	0.60	0.12	0.04	0.017	18.0
HUL2	64.07	9.89	3.86	2.27	5.48	1.07	2.37	0.50	0.16	0.06	0.011	10.1
HUL2	63.37	10.17	3.76	2.25	5.98	1.06	2.43	0.46	0.12	0.06	0.009	10.2
HUL3	54.51	14.35	5.17	2.92	4.51	1.03	2.76	0.63	0.13	0.05	0.015	13.8
HUL3	38.95	11.06	3.98	6.53	15.02	0.87	2.28	0.49	0.10	0.05	0.011	20.4
JAR1	51.71	13.18	4.97	3.54	6.86	1.04	2.71	0.58	0.12	0.10	0.015	15.0
JAR1	50.71	13.55	4.98	3.30	7.33	1.05	2.86	0.61	0.12	0.07	0.016	15.2
KRO1	54.44	13.89	5.12	3.11	5.91	1.06	2.77	0.68	0.11	0.06	0.015	12.6
KRO1	65.51	11.99	4.51	1.31	1.06	1.27	2.27	0.64	0.15	0.04	0.011	11.1
KRO1	50.07	12.11	5.03	3.33	7.68	0.88	2.47	0.52	0.14	1.71	0.014	15.9
KRO1	60.32	9.76	3.64	3.11	7.43	1.27	2.04	0.62	0.15	0.07	0.011	11.4
KRO2	50.16	13.31	4.87	3.56	8.31	1.08	2.65	0.60	0.11	0.06	0.016	15.1
KRO2	53.27	13.34	4.96	3.40	6.54	1.02	2.68	0.60	0.11	0.05	0.014	13.8
KRO2	66.89	7.32	2.56	2.73	7.15	1.07	1.68	0.46	0.10	0.05	0.009	9.8
KRO2	60.45	12.57	4.52	2.85	3.97	1.09	2.70	0.58	0.11	0.06	0.014	10.9
SLU1	52.45	13.28	4.80	3.70	7.10	1.03	2.95	0.60	0.14	0.07	0.015	13.7
SLU1	53.34	11.68	4.39	3.13	9.74	1.27	2.26	0.64	0.14	0.07	0.013	13.2
SLU1	61.20	9.59	3.78	2.38	8.85	1.34	1.76	0.50	0.14	0.07	0.009	10.2
SLU1	50.03	15.48	5.83	3.52	7.23	1.25	3.16	0.72	0.14	0.07	0.016	12.3
TL1	59.70	7.54	3.44	3.40	9.58	1.16	1.53	0.58	0.12	0.07	0.010	12.7
TL1	61.80	6.87	3.13	3.21	9.43	1.14	1.47	0.46	0.11	0.06	0.010	12.2
TL1	52.58	12.91	4.78	3.65	7.40	1.13	2.69	0.58	0.14	0.07	0.013	13.9
TL2	52.09	12.71	4.69	3.00	8.04	0.99	2.54	0.57	0.13	0.06	0.015	15.0
TL2	56.52	10.97	4.14	3.12	7.36	1.13	2.26	0.53	0.13	0.07	0.013	13.6
TL2	53.61	12.01	4.60	3.37	8.36	1.12	2.45	0.59	0.11	0.08	0.015	13.5

Electronic supplement

Appendix 2: The trace element composition (ppm) of the studied samples.

Sample (borehole)	Ni	Sc	Ba	Co	Nb	Rb	Th	U	V	Zr	Y	La
BAR1	42	11	319	9.2	11	107.2	8.5	2.5	109	133.1	19	27.1
BAR1	59	11	308	9.6	10.6	112.5	9.4	2.3	117	107.2	18.9	26
BAR1	69	14	449	10.4	10.2	136.3	11	5.5	185	144.4	24.3	31
BAR1	49	11	308	9.6	9.3	99.1	9.1	2.6	101	124.5	18.1	26.5
G1	14.7	4	203	4.2	7	40	3.5	1.8	32	68.9	12.6	11.3
G1	52.8	15	465	15.2	16.4	154.3	12.5	3.7	151	187.2	26.1	34.6
G1	15.3	6	210	4.9	8.2	43.5	4.4	1.8	37	123.3	16.9	17.2
G1	12.7	4	281	4.4	8.6	32.1	4.8	1.7	30	148.7	15.9	17.8
G1	46.9	13	479	14.6	14.6	145.6	11.1	3.4	150	164.9	24.6	35.5
G1	10.5	5	194	4.2	7.4	37.5	3.3	1.2	29	124.7	13.3	12.5
G2	58	14	565	13.1	11.8	153.7	11.1	6.4	233	103.2	22.9	33.1
G2	65	13	577	11.6	11.7	152.4	10.8	12.9	226	108.4	23.3	33.9
G2	58	17	474	17.6	16.8	178.7	13.7	3.7	181	164.6	26.8	43.5
G2	59	15	671	15.8	13.7	169.2	12.4	6.7	227	117.5	25.8	36.8
G2	56	15	471	18.1	14.8	173.1	13.1	4.4	196	136.1	26.7	40.2
G2	59	13	597	11.7	12.2	148.9	10.3	12.3	217	111.5	24.2	35.3
G2	74	18	488	16.4	16.1	234.1	14.6	4.8	205	151.2	29.7	46.2
G2	102	15	578	21.9	12.5	169.3	11.3	15.2	341	110.2	25.3	36.2
G3	63	16	466	15.9	16.6	182.6	13.8	3.7	171	144.5	27.4	38.9
G3	58	14	422	14.8	13.7	144.8	10.9	2.9	134	169.3	22.5	31.9
HOL1	83	14	416	13.8	11.7	134.1	10.2	6.6	244	104.3	19.9	27.6
HOL1	57	13	386	11.7	15.1	147.1	11.3	3.2	146	120.7	22.8	32.1
HOL1	38	7	313	7.2	7.5	178.3	6.1	1.8	69	131.8	18.6	21.3
HOL1	44	10	354	9	8.4	106.3	10.2	2.8	105	172.7	19.7	27
HOL1	48	10	374	9	7.8	109	9.6	2.9	110	160.1	18.3	27.8
HOL1	47	10	351	8.6	9.6	101.5	9.4	3.1	97	182.9	19.5	27.3
HOL1	59	12	368	10.9	9.8	125.1	11	3.2	123	144.4	20.9	29.7
HOL1	25	6	1505	4.8	4.8	55	4	1.4	47	108	16.7	21.5
HOL1	35	7	362	8.1	6.5	78.3	8.5	2.9	71	191.8	24.1	24.4
HOL1	62	13	355	11.3	11.9	130.9	10.3	3.1	139	120.7	19	28
HOL1	35	7	2044	9	6.3	70	5.5	2.0	65	134.7	17.9	20.5
HUL2	44	10	438	9.4	11.2	113	9.3	2.9	100	186	21	26.2
HUL2	74	13	422	10.4	11.4	137.9	9.5	6.3	296	93.9	18.4	25.7
HUL2	45	8	458	9.2	10.4	95.1	11.5	3.3	77	262.1	24.5	33.7
HUL2	42	8	458	9	8.3	94.1	9.1	2.7	82	174.4	18.3	24.9
HUL3	54	13	317	11.8	12.7	136.8	10.1	3.6	138	116.7	18.7	28
HUL3	48	10	287	8.7	8.4	107.1	9.4	3.7	106	109.1	18.8	25.7
JAR1	48	12	324	11.9	10.8	131.5	9.5	2.9	128	115.1	17.9	25.4
JAR1	53	12	333	11.2	12	134.6	9.3	2.8	138	105	19.5	26.7
KRO1	56	12	396	11.4	12.5	136.5	10.7	3.3	138	164.8	23.3	31.6
KRO1	54	10	387	12.7	10.7	104.5	8.8	9.1	114	179.7	20	24.7
KRO1	59	11	339	20.3	9.5	115.1	9.5	2.4	124	100.6	18	26.5
KRO1	34	8	384	9.2	9.8	78.6	9.8	2.9	76	265.3	21.6	28.1
KRO2	58	11	366	12.5	13.2	136.9	10.1	3	127	123.2	22.7	29.1
KRO2	92	11	361	10.3	11.2	130.5	10.6	3	126	132.5	19.1	29
KRO2	31	7	289	6.5	8.1	66.5	6	1.9	60	194.1	17.2	19.5
KRO2	65	10	401	12.2	10.4	118.6	10.5	2.9	117	159.5	21.9	28.2
SLU1	36	12	383	11.8	11.8	143.2	10	3.2	131	113.4	20.7	31.7
SLU1	37	10	355	12	12.7	104.8	9	2.8	105	174.7	23.6	30.4
SLU1	24	8	312	8	9.6	74.1	6.9	2.0	81	162.7	24.5	26.1
SLU1	53	14	468	15.7	15.6	154.4	12.9	3.8	173	160.3	25.8	37.9
TL1	27	7	312	7	9.9	61.1	5.5	1.9	57	144.3	16.1	18.4
TL1	24	6	309	6.4	8.1	56.9	4.6	1.5	50	119.7	13.7	15.4
TL1	46	12	318	11.1	11	127	8.8	3	117	111.8	19.6	25.5
TL2	59	12	311	10.9	11.7	126	9.2	3.9	154	106.2	19.6	25.1
TL2	41	10	312	3.12	10.1	105	8	2.2	96	113.9	18.6	23.5
TL2	51	11	314	9.1	10.1	102.6	8.6	2.3	101	124	18.9	24.3